THESIS REPORT

Master's Degree

Investigation of Wheel Wear and Its Effect on Forces Encountered in Grinding of Silicon Nitride

by K.T. Ritchie
Advisor: G.M. Zhang

M.S. 96 -9

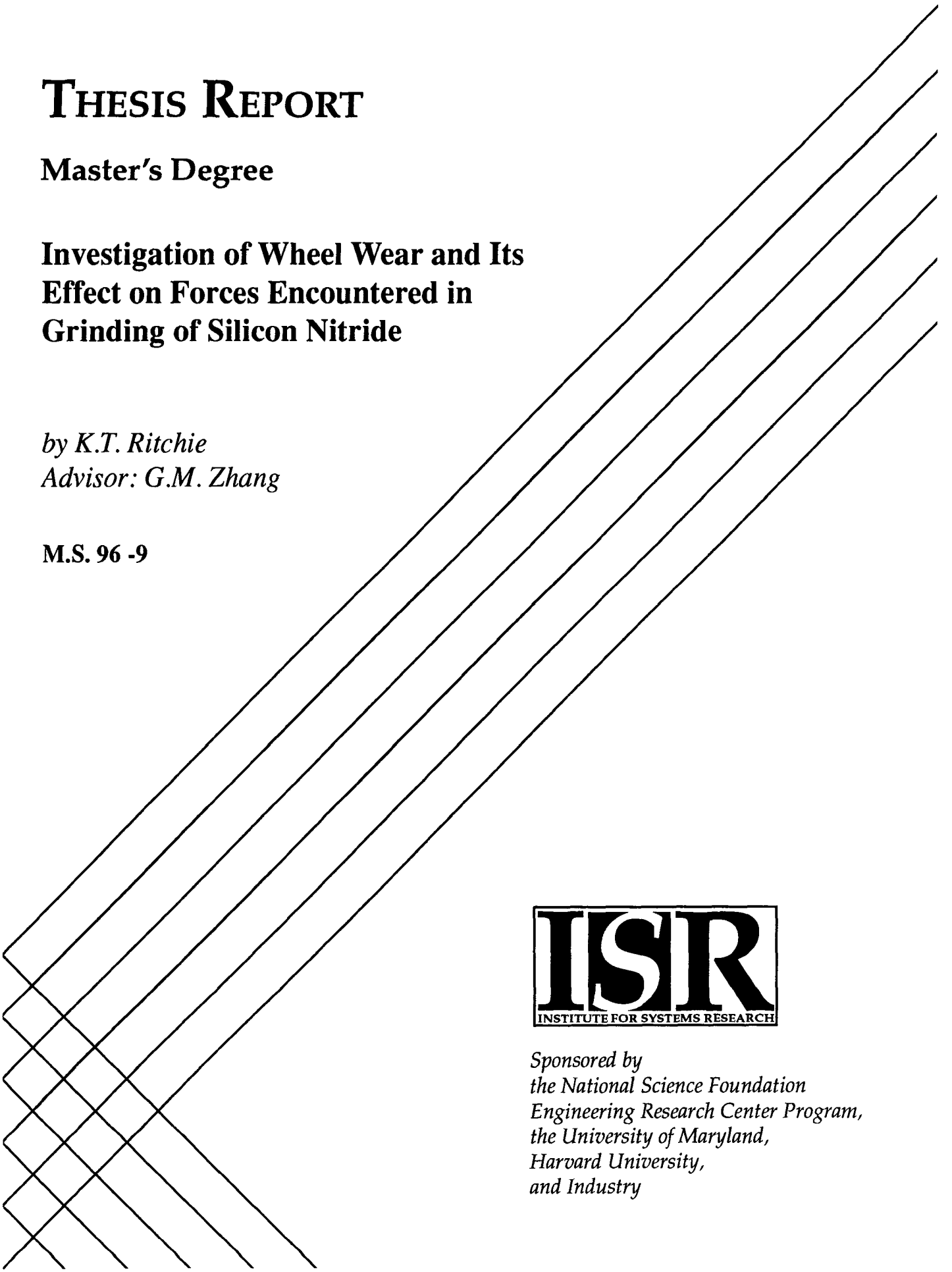

Sponsored by
the National Science Foundation
Engineering Research Center Program,
the University of Maryland,
Harvard University,
and Industry

Abstract

Title of Thesis:	INVESTIGATION OF WHEEL WEAR AND ITS EFFECT ON FORCES ENCOUNTERED IN GRINDING OF SILICON NITRIDE
Name of degree candidate:	Kevin Thomas Ritchie
Degree and Year:	Master of Science, 1996
Thesis directed by:	Associate Professor Guangming Zhang Department of Mechanical Engineering & Institute for Systems Research Dr. Said Jahanmir National Institute of Standards and Technology

A necessary goal in the study of grinding advanced ceramic materials is to define grinding conditions that will machine ceramic components economically while maintaining dimensional accuracy and surface integrity of the resulting parts. In view of the high price of diamond wheels, which are the optimum choice for machining ceramics, it is important to investigate the process of diamond-wheel wear in grinding ceramic materials. Little information is currently available on the rates of diamond-wheel wear in grinding ceramic materials.

This thesis proposes a new method of measuring wheel wear using a duplication pattern of the grinding wheel. Plunge-grinding experiments on sintered silicon nitride (SSN) and sintered reaction-bonded silicon nitride (SRBSN) were conducted using a horizontal-spindle surface grinder with diamond-grit, resin-bond peripheral wheels. To gain a better understanding of the wear process, grinding forces were measured using a

computer-based data-acquisition system. Stylus profilometry served to measure the volumetric wheel wear and to measure the surface roughness of the ground silicon nitride for the purpose of characterizing the effect of wheel wear on the grinding performance. Major contributions of this thesis research include development of a method for measuring wear of diamond grinding wheels, and identification of the interrelation between the rate of wheel wear and the two machining parameters (namely, downfeed and wheel speed used in the investigation).

INVESTIGATION OF WHEEL WEAR AND ITS EFFECT ON FORCES ENCOUNTERED IN GRINDING OF SILICON NITRIDE

by

Kevin Thomas Ritchie

Thesis submitted to the Faculty of the Graduate School
of the University of Maryland in partial fulfillment
of the requirements for the degree of
Master of Science
1996

Advisory Committee:

Associate Professor Guangming Zhang, Chairman/Advisor
Associate Professor Isabel Lloyd
Associate Professor James Sirkis
Dr. Said Jahanmir, Advisor
National Institute of Standards and Technology

DEDICATION

This work is dedicated to my Grandpa, the first engineer I knew.

ACKNOWLEDGMENTS

The author wishes to express his sincere and profound gratitude to Dr. Said Jahanmir, supervisor of this research and member of the advisory committee, and to Dr. Guangming Zhang, chairman of the advisory committee, for their constant inspiration and support, invaluable guidance, and helpful assistance throughout this research. Sincere gratitude also goes to Lewis Ives for his kind guidance and generous assistance in this research. I would also like to thank Dr. Isabel Lloyd and Dr. James Sirkis for serving on my advisory committee.

The author would like to express his cordial thanks to Lenox Job for his help in setting up the force-measurement system. The author gratefully acknowledges Dr. Hockin Xu for many fruitful discussions. Thanks are extended to Eric Ives for his assistance in manufacturing pieces of the experiment apparatus.

Finally, the author must thank his parents and family for their constant support and encouragement.

TABLE OF CONTENTS

LIST OF TABLES

LIST OF FIGURES

Chapter 1

Introduction

Advanced ceramic materials have found increasing use in industrial applications because of the superior thermal, chemical, and wear-resistance characteristics of ceramics as compared to those of traditional materials. However, a primary obstacle to the use of ceramics for many applications is the high cost of machining these hard materials. Recent research in the field of ceramic machining has focused on the information needed to develop creative and cost-effective machining technologies.

Diamond-cutting tools -- specifically, diamond-grit grinding wheels -- are needed in machining ceramics because of the high hardness of the materials. The high price of diamond grinding wheels -- the expense associated with using diamond materials, and the costs of wheel conditioning (e.g., trueing and dressing) -- makes affordable machining of ceramics difficult. This thesis addresses the problem of economical machining of ceramic components by studying grinding conditions that minimize wear on the diamond grinding wheel.

Of all machining processes, grinding is unmatched for most precision operations. Grinding provides the accuracy and surface finish required for machining materials like advanced ceramics, whose strength and part integrity are highly sensitive to machining damage and to post-machining surface conditions. The current requirement for grinding

machines is that they should not only machine these "hard-to-grind" ceramic materials but also produce a workpiece with precise dimensions and quality surfaces.

Grinding was once considered a mere stock-removal process; finish grinding was highly discouraged for large stock-material removal operations, because it cost more than did other machining processes per unit volume of material removal. However, recent near-net shape-processing techniques have reduced the amount of material removal needed in finish-machining processes, increasing the attractiveness of grinding as a single machining process capable of achieving final dimensions.

1.1. Motivation and Background

The absence of data on finishing techniques for ceramic materials is a key technological barrier preventing widespread use of advanced ceramic materials. Proper selection of grinding-process parameters and grinding-system variables can result in ceramic materials of high strength and superior surface finishes. Ceramic materials with high-density/high-strength properties would be desirable as cutting tools and bearings, and for use in high-temperature/high-density automotive applications.

Use of advanced ceramics has been limited by the lack of reliable data on performance, cost-effective machining processes, and tooling cost. At present, producing ceramic materials with quality surface finish is a slow and cost-intensive process. Surface damage caused by machining produces a material of compromised

structural integrity, further decreasing the attractiveness of using advanced ceramics in engineering applications.

1.2. Scope of Study

The objective of this research is to study the wear process of diamond-grit wheels during grinding and the influence of diamond-grit wheel wear on the forces and surface finish produced in grinding silicon nitride ceramics. Test methods for measurement of wheel wear and grinding forces were established for this research work. These experiments have permitted evaluation of the effect of machining conditions on wheel wear during grinding of sintered silicon nitride (SSN) and sintered reaction-bonded silicon nitride (SRBSN). Measurements of grinding-wheel wear, grinding forces, and the surface roughness of the ground workpieces were combined to determine the effect of wheel wear on grinding ceramic materials.

1.3. Organization of Thesis

The next four chapters of this thesis describe the constituents of this research. Chapter Two: Background & Literature Review is an overview of previous work on the problem. Chapter Three: Experiment Procedure describes the steps involved in conducting wheel-wear experiments. Chapter Four: Results contains the analysis of the experimental data and discusses the results. Chapter Five: Conclusions and Recommendations sets forth the major findings of this research and offers suggestions for further study.

Chapter 2

Background & Literature Review

This literature survey assembles data on the effect of diamond-wheel wear on the grinding of silicon nitride ceramics. The high cost of machining and finishing advanced ceramics has been a major barrier to the use of ceramics in commercial applications [Jahanmir et al., part I 1993]. The effect of wheel wear on grinding performance has previously been studied for non-diamond wheels (e.g., aluminum oxide grinding wheels used to grind metallic materials) [Malkin and Cook, part 1 1970, Kirk 1976]. Less information exists on the physical interaction of diamond particles with ceramic materials [McEachron and Lorence 1988, Gangopadhyay and Tamor 1993].

This summary includes an overview of the grinding of ceramics, grinding forces, surface roughness, and wheel wear. Wheel wear not only serves as a measure of a diamond grinding wheel's tool life, but also may influence (decrease) the strength of the workpiece produced, because of its effect on surface condition and integrity of the machined ceramic surface. The high hardness of ceramic materials requires higher grinding forces during the material removal process that accelerate wear on the diamond cutting edges and confirm ceramics as difficult-to-machine materials [Tsutsumi et al. 1993].

2.1. Grinding Process

The grinding process makes use of cutting tools composed of a large number of abrasives held together by a bond (e.g., grinding wheel). One advantage of grinding is that it can be used to machine a workpiece to an accurate size and produce a quality surface finish. The abrasive grains in the wheel penetrate the workpiece surface and cut away material softer than the abrasive material itself. Diamond abrasives have been used extensively in grinding hard materials such as ceramics [Malkin 1989].

Grinding is a dynamic procedure involving the grinding machine, the grinding wheel, and the workpiece. A frequently overlooked factor in the grinding process is the machine. Also, the machine operator may be one of the key uncontrollable variables, because each operator brings unique skill, knowledge, and ability to the grinding process. Two time-related factors that ultimately affect workpiece accuracy and surface finish are wheel wear and wheel conditioning. Note that wheel wear consists of the combination of wear of the grit and wear of the bond (or matrix) [Malkin 1989].

Trueing is "the generation of a geometrically correct wheel face with minimum wheel runout" [Subramanian and Keat 1985]. The purpose of wheel trueing is to minimize surface runout of the grinding-wheel face. Dressing is "the operation which modifies the wheel surface topography to protrude the grain cutting edges from the bond surface." Often aluminum oxide or silicon carbide is used to "dress" a resin-bond diamond grinding wheel [Inasaki 1989]. Some "self-dressing" occurs during mechanical

fracture of the grains and bond bridges, resulting in new cutting edges and improved cutting ability [Yoshikawa and Sata 1963].

The demand for effective grinding and finishing of ceramic materials has increased with the development and use of these materials [Gagliardi 1992]. Ceramic materials are desirable because of their high hardness, high strength, wear resistance, and thermal properties [Kitajima et al. 1992, Ives et al. 1993]. Components made of ceramic material offer improved performance and better efficiency compared to metals; however, ceramic materials are sensitive to surface and subsurface damage incurred during grinding, and their behavior under loads is affected by machining damage [Hu and Chandra 1993].

2.2. Grinding Forces

Numerous investigators have measured and interpreted the tangential and normal force components of the grinding process [Story 1968]. Generally, forces measured in surface-grinding are of three linearly-independent directions: normal, tangential, and transverse (i.e., crossfeed). The normal grinding force in ceramic grinding is generally greater than the tangential or the transverse force. As the diamond particles loosen with wear, the ratio of normal force to tangential force decreases compared to that of a wheel of better bonded, less worn diamonds [Busch and Prins 1970]. Flattening of the abrasive grains with wear requires use of higher normal forces if the flatter crystals are to penetrate into the workpiece during grinding [McEachron and Lorence 1988]. Damage

to the ceramic material, including changes in its microstructure, will be proportional to the mechanical forces applied during grinding [Spur et al. 1985]. Using a conservative approach to grinding of ceramics will normally minimize the potential damage caused by grinding [Jahanmir et al., part I 1993].

2.3. Surface Quality

Surface quality is often a critical factor in the reliability of a machined part. Surface quality consists of the surface finish (i.e., "topography of the machined surfaces") and surface integrity (i.e., "mechanical or metallurgical alterations to the surface layer induced by machining") of the workpiece [Malkin 1989]. The fundamental problem in working with ceramic materials is the micro- and macrocracking produced in the grinding process; these induced cracks affect the flexural strength of brittle materials [Spur et al. 1985]. An experiment testing the effect of surface condition on the flexural strength of sintered silicon nitride suggests that grinding damage will decrease the strength of the material [Ovri and Davies 1987].

Roughness of the surface immediately following dressing of the diamond wheel is generally high, decreases to a steady-state value, then increases sharply as the wheel becomes dull [Peters et al. 1982]. Experiments show that average surface roughness, R_a, increases with increasing the grit size of the grinding wheel [Tsutsumi et al. 1993]. For example, a fine 10000-grit (2 μm) grinding wheel produces a surface roughness, R_a, of

0.01 μm, whereas the surface roughness produced by a 140-grit (100 μm) grinding wheel is ten times greater.

2.4. Grinding Wheels and Fluids

Grinding wheels consist of abrasive grains, often called grits, and the bonding material that holds the grains together. Diamond is the preferred superabrasive grit material for machining ceramic materials because of its superior hardness. The diamond abrasive grains are attached to the grinding wheel by various kinds of bond materials. Three bond materials (resinoid, vitrified, and metal) are used to produce superabrasive wheels for cutting ceramics, stone, and other hard brittle materials. Resinoid-bonded wheels, the most popular superabrasive wheels, are produced by mixing the abrasive grit with thermosetting resins, molding to shape, and curing (baking) the wheels. Vitreous-bonded wheels are created from mixtures of clay, feldspar, and a frit; the mixture is shaped, dried, and then fired in a kiln. Metal-bonded and electroplated wheels are commonly produced from sintered bronze via powder-metallurgy methods [Malkin 1989].

Heat and friction are byproducts of the grinding process that adversely affect the accuracy of the workpiece, surface finish, and wheel wear. When workpiece accuracy and surfaces with high quality finish are required, the workpiece is wet-ground using one of three main kinds of grinding fluids: water-soluble oils, water-soluble chemicals, and straight oils. Straight oils (i.e., mineral oils, paraffin oils, and synthetic oils) are

petroleum or vegetable-based oils that are widely used for metal-forming and low-speed metal-cutting operations. Water-soluble oils contain emulsifiers to permit the formation of a stable mixture of oil in water. Water-soluble oils are used for more severe metalworking applications. Water-soluble chemicals (or chemical emulsions) generally mix more easily into water than do soluble oils; otherwise, they differ little from soluble oils. Another importance function of the grinding fluid is to remove debris from the workpiece during machining [Byers 1994].

2.5. Wheel Wear

Wear on a grinding wheel is an unavoidable result of the grinding process. However, the amount of wear can be minimized by properly matching wheel type to the material being ground. For instance, wear on a diamond-grit grinding wheel will be less than that on an aluminum oxide wheel when grinding advanced ceramics, because the hardness of diamond is relatively higher than that of aluminum oxide. Parameters of the grinding process (downfeed, table speed, and grit size) will also significantly affect wheel wear. Proper choice of these parameters can be determined experimentally. Wheel wear can be quantified by the volumetric loss of material from the grinding wheel during grinding. For plunge grinding (i.e., grinding with the absence of a crossfeed motion of the workpiece relative to the grinding wheel) the volume of radial wheel wear is:

$$V_s = \pi d_s \Delta r_s b$$

where V_s is the radial wheel-wear volume; d_s is the mean of the wheel diameters (before-and-after grinding); Δr_s is the change in the wheel radius; and b is the grinding width [Malkin 1989]. The grinding ratio, commonly referred to as the G-ratio, is a performance index used to characterize the grinding wheel's resistance to wheel wear. The grinding ratio G is defined as

$$G = \frac{V_w}{V_s}$$

where V_w is the volume of workpiece material removed and V_s is the radial wheel-wear volume [Malkin 1989]. A G-ratio of 100 means that the grinding wheel removes 100 units of workpiece material for each unit of volume that the wheel wears.

Grinding of metals produces two forms of grinding-wheel wear: attritious, and fracture [Malkin and Cook, part 1 1970]. Attritious wear in metal grinding (dulling of the wear flats on the surface of the wheel) is linearly related to the normal and tangential grinding forces. The amount of fracture wear, directly related to the G-ratio (defined as the volume ratio of ***metal*** removed to wheel wear), indicates the efficiency of the grinding process. The main goal of this research is to quantify the wheel wear and to show the effect of diamond-grit wheel wear on grinding forces and G-ratio in grinding ceramic materials.

Optimal grinding parameters would result in high stock removal from the workpiece but would not require frequent dressing of the diamond-grit wheel. Grinding parameters (including table speed, downfeed, and wheel speed) are well understood, but

wheel-wear rate and surface damage need to be quantitatively examined [Hahn 1993]. Understanding grinding-wheel tool life would prevent premature dressing of the grinding wheel and decrease damage to the workpiece [Brinksmeier et al. 1992].

Chapter 3

Experiment Procedure

The focus of this thesis is the wear of diamond-grit grinding wheels and its effect on forces encountered in grinding of silicon nitride. This chapter provides information on the grinding machine, preparation of the wear specimens, force-measurement system, and wheel-wear measurement procedure used for this research. This chapter also includes a description of the three sets of experiments to investigate wheel wear and its effect on grinding forces.

3.1. Grinding Machine

In this study a reciprocating-table, horizontal-spindle surface grinder was used to measure the wear of a diamond-grit grinding wheel. Surface grinding is usually employed to produce flat surfaces by using either the periphery or face of a grinding wheel. Periphery-surface grinding is the preferred method for precision grinding as it offers excellent control of workpiece size and geometry.

Wheel-wear experiments were performed on an instrumented Chevalier FSG818 AD precision grinding machine; a digital readout displayed the crossfeed and vertical location of the grinding spindle in reference to the worktable. A precision ball-bearing spindle fitted to the grinding machine before beginning the wear experiments has

a feedback controller to maintain a constant and precise wheel speed during the experiments.

To ensure consistent results among the grinding experiments, the used grinding fluid in the coolant reservoir with replaced with new grinding fluid; this removed any possible contribution to wheel wear of diamond (or other) particles from a previous experiment in the used coolant. The presence of foreign particles in the grinding fluid might accelerate wear on the grinding wheel, resulting in inaccurate wheel-wear rate measurements. The grinding fluid used in this experiment was Cincinnati Milacron Cimperial HD-90, a "heavy-duty" fluid (a water-soluble oil-based emulsion prepared in a 20:1 dilution with water) recommended for grinding ceramic materials.

3.2. Design and Preparation of the Samples

Three silicon nitride ceramics were used in this experiment -- sintered silicon nitride (SSN), reaction-bonded silicon nitride (RBSN), and sintered reaction-bonded silicon nitride (SRBSN). SSN and SRBSN have similar mechanical properties; their densities are greater than that of reaction-bonded silicon nitride, and their porosity is less than 1%. Table 3.1 is a comparison of properties of these selected silicon nitride ceramics.

Table 3.1. Properties of Silicon Nitride Ceramics [Ives 1993]

Material	SRBSN	SSN	RBSN
Composition	AL_2O_3 & Y_2O_3	----	----
Density (g/cm^3)	3.22	3.20*	2.36
Porosity	< 1 %	----	20 %
Alpha-to-beta ratio	All Beta	All Beta	7.7: 1
Grain size Length x width (μm)	6-8 x 1-3	0.3 - 1.3**	1-2 x 0.5-1
Elastic modulus (GPa)	300	306	200
Fracture strength (MPa)	674	668	205
Fracture toughness, K_{IC} (MPa $\sqrt{m}$)	2.5	6.8***	2.5
Vickers hardness (GPa)	----	14.2 ± 1	6.8 ± 0.7

* > 99% theoretical density
** Grains have 1:4 aspect ratio (i.e., length-to-width ratio of the grains).
*** Chevron notch test

The preliminary wear experiments used SSN and SRSBN test specimens measuring 3mm thick, 4mm wide, and 50mm long ($600mm^3$), dimensions corresponding to the ASTM C1161 standard for B-size 4-point flexure specimens. The preliminary wear experiments indicated that more material needed to be ground to observe the wear-curve transition from the initial to accelerated wear stages. Larger sintered reaction-bonded silicon nitride (SRBSN) test specimens were specifically prepared to cause greater wear on the diamond-grit grinding wheel. These SRBSN bars of rectangular shape had approximately three times more volume than that of the SSN and SRBSN four-point bend-bar wear specimens used in preliminary wear experiments. Nominal dimensions of these bars were 3mm thick, 7mm wide, and 83mm long ($1743mm^3$). The bars were sliced from a billet 7mm in thickness, 82mm in width, and 84mm in length by an Aremco ACCU-CUT 5200 dicing saw using Cimperial HD-90 grinding fluid in a 20:1

concentration with water. The cutting blade was a 4-inch-diameter diamond-tipped 20μm thick wheel. Figure 3.1 compares the wear specimen used in this experiment (left figure) and the smaller four-point bend bar used in the preliminary experiments (right figure).

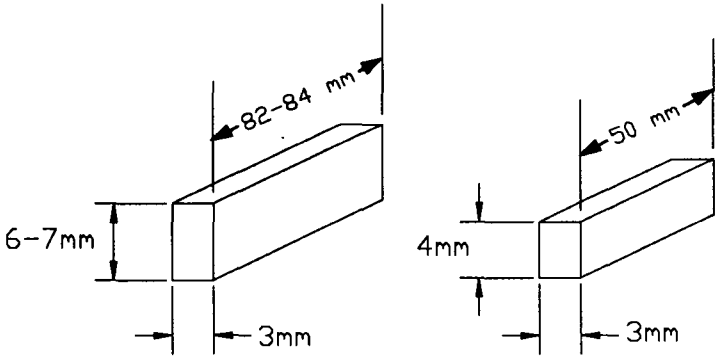

Figure 3.1. Comparison of Wear Specimen (left) and Four-Point Flexure Bar (right)

3.3. Mounting of Specimens

The attachment and alignment of the ceramic specimens to the mounting plate were important aspects of the experiments. Special attention was needed to ensure that each bar remained fixed to the mounting plate during the bar's exposure to each machining condition. Figure 3.2 shows the wear specimens attached to the steel mounting plate. The ceramic samples were attached by a thin layer of superglue (cyanoacrylate) to a steel mounting plate. Superglue was the adhesive chosen for superior strength under the high-force/high-temperature conditions of grinding.

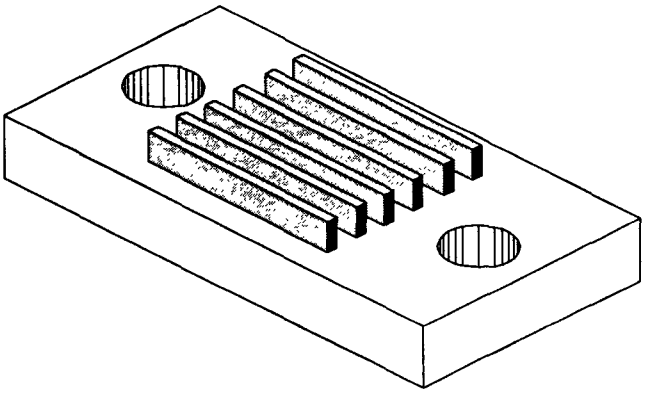

Figure 3.2. Mounting of SRBSN Specimens

The wear specimens were spaced 0.5 mm apart to maximize the number that could be mounted on the steel plate, and to provide the clearance between bars needed to ensure that only one bar would be in contact with the wheel during each grinding pass. The bars were mounted as nearly parallel to each other as possible to simplify alignment of the bars with the wear groove formed in the grinding wheel. A dial indicator permitted alignment of the wear specimens and the grinding wheel within 5 μm of parallel.

The first step in the wear experiment was to align the first silicon nitride specimen parallel to the grinding wheel. A dial indicator was mounted to the housing around the grinding wheel and the grinding table translated in the crossfeed direction until the stylus of the dial indicator touched the outside edge of the specimen. The indicator was then used to check the relative distance of the specimen to the grinding wheel, by translating the grinding table in the tangential direction and monitoring the indicator displacement. Slight adjustment to the orientation of the mounting plate permitted proper alignment of the wear specimens with respect to the wheel. Figure 3.3

shows wear specimens properly aligned with the grinding wheel (left figure) and specimens improperly aligned with the grinding wheel (right figure).

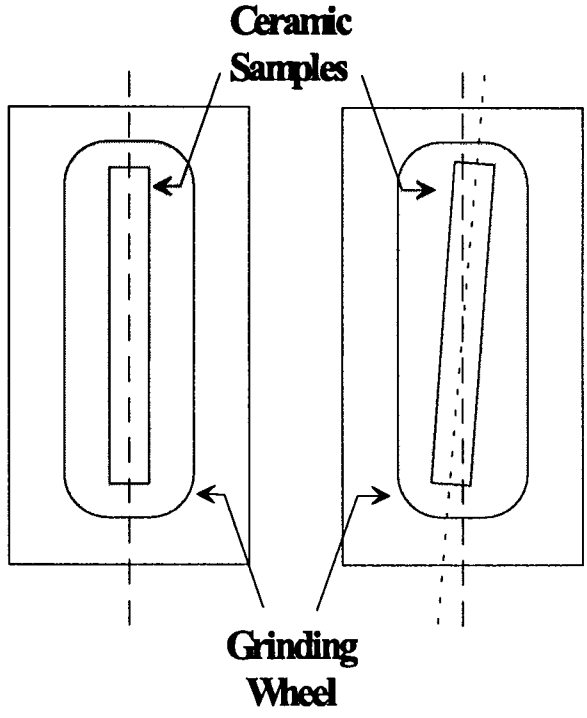

Figure 3.3. Proper (left) and Improper (right) Alignment of Wheel-Wear Specimens to the Grinding Wheel

The next step was to position the wear specimen under the center of the wheel, to keep the wear groove in the same place on the grinding wheel. The grinding wheel was lowered to a position below and behind the first bar to be ground. With care, the wheel was moved in the crossfeed direction to a point where the side of the grinding wheel and the side of the wear bars just began to touch. The digital readout was used to relocate the grinding wheel at the center of the wear bar from the datum position.

The final step was to lower the grinding wheel (using the manual downfeed controls) to the point where the grinding-wheel grit engaged the top of the workpiece to be ground. The digital readout in the normal direction was zeroed, and the wear specimen was ready to be ground.

3.4. Wheel Preparation: Trueing and Dressing Procedure

Trueing and dressing of the grinding wheel are key elements in the proper grinding of ceramics. Before grinding experiments began, the grinding wheel was brake-trued using silicon carbide wheels and dressed using an alumina dressing stick. Brake-trueing of the wheel was performed to make the wheel concentric. The grinding-wheel speed during the brake-trueing procedure was set to the same wheel speed to be used in the wear experiments; i.e., the wheel speed was set at 3600 rpm for the 8-inch wheels used in the preliminary wear experiments, and at 3756 rpm for the 6-inch wheels used in the effect-of-downfeeds experiments. Brake-trueing was performed using three downfeeds, each successive downfeed smaller than its predecessor. A 25-μm downfeed was initially selected. The total downfeed for the 25-μm downfeed ranged from 5 mm to 10 mm. A 10-μm downfeed was then used for a total downfeed ranging from 3 mm to 6 mm. The final downfeed of 5-μm was used for a total downfeed ranging from 2.5 mm to 5 mm until the wheel was sufficiently trued. Profiles of the grinding wheel were ground into a soft glass specimen, profile measurements of which served to determine when the grinding wheel was properly trued. (The grinding wheel was considered properly trued when the profile trace became flat and the peak-to-valley distance became minimal.) The

wheel was dressed using 16.4 cm^3 of an alumina dressing stick following the trueing process.

3.5. Force-Measurement System

A data-acquisition instrument was used to monitor and record normal and tangential grinding forces. The four primary components of the measurement system were a Kistler quartz-type 9257B 3-component piezoelectric dynamometer, a set of three Kistler 5004 dual-mode charge amplifiers, a Keithley data-acquisition screw-terminal accessory board, and a 486DX Gateway 2000 computer running the Keithley Viewdac data-acquisition software.

Figure 3.4 shows the components and orientation of the periphery-surface grinder and grinding-force measurement system. A Hewlett Packard 54601A oscilloscope verified the input and output sources through the system. The force-measurement system collected and recorded the three force components -- normal, tangential, and transverse -- applied to the ceramic workpiece during the grinding process.

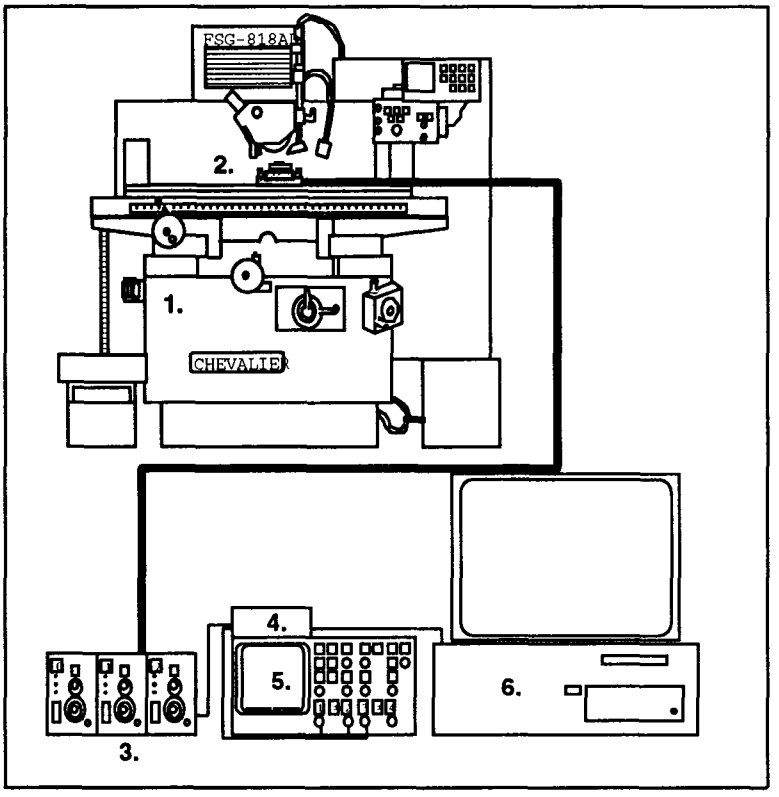

Equipment:

1. *Chevalier* FSG-818 AD grinding machine
2. *Kistler* quartz-type 9257B 3-component dynamometer
3. *Kistler* Model 5004 dual-mode charge amplifiers
4. *Keithley* data-acquisition screw terminal accessory board
5. *Hewlett Packard* Model 54601A oscilloscope
6. *Gateway 2000* 486 computer

Figure 3.4. Periphery Surface Grinder and Force-Measurement System

Figure 3.5 shows the steel mounting plate attached to the dynamometer. The steel mounting plate holding the ceramic samples was rigidly attached to the piezoelectric dynamometer, which had been secured to the worktable. Grinding force applied to the workpiece was transmitted to the piezoelectric transducer, which emits charge signals corresponding to the different force directions; these signals were amplified and converted to voltage signals with the aid of the charge amplifiers. In turn, the data-acquisition hardware was used to obtain the grinding-force data. Finally, the

grinding data were stored on the personal computer for further manipulation. An attached oscilloscope provided a second method of visually monitoring the analog-force signals.

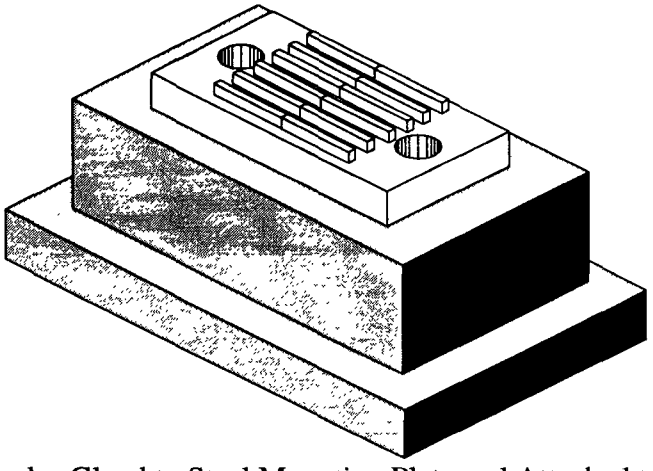

Figure 3.5. Samples Glued to Steel Mounting Plate and Attached to Dynamometer

A commercial software package -- Keithley VIEWDAC -- was used to acquire and record data from the data-acquisition hardware. To accomplish these two tasks, a data-acquisition program was written. Figure 3.6 shows the program flowchart, with the data- acquisition code subdivided into five subroutines: Conversion, Go (Toggle Button), Loop 1, Save, and Write. The first subroutine, Conversion, allows the user to customize the data-acquisition sampling frequency depending on the duration of the grinding tests, or to compensate for any aliasing that might occur. The second subroutine, Go, is a toggle button that initiates and terminates the data-acquisition loop. The third subroutine, Loop 1, acquires three channels of data at the specified sampling frequency, creates three data sets, stores the data in the memory buffer, and plots them on the computer screen. The fourth subroutine, Save, displays a panel prompting the

user to save data sets with a given filename in a particular location: e.g., in a directory on a disk, or on the computer's hard drive. In addition, the Write subroutine records the three data sets created by Loop 1 with the indicated parameters (filename and location) in ASCII format. Appendix A lists the complete data-acquisition code. Appendix B shows the procedure involved in the data- acquisition system.

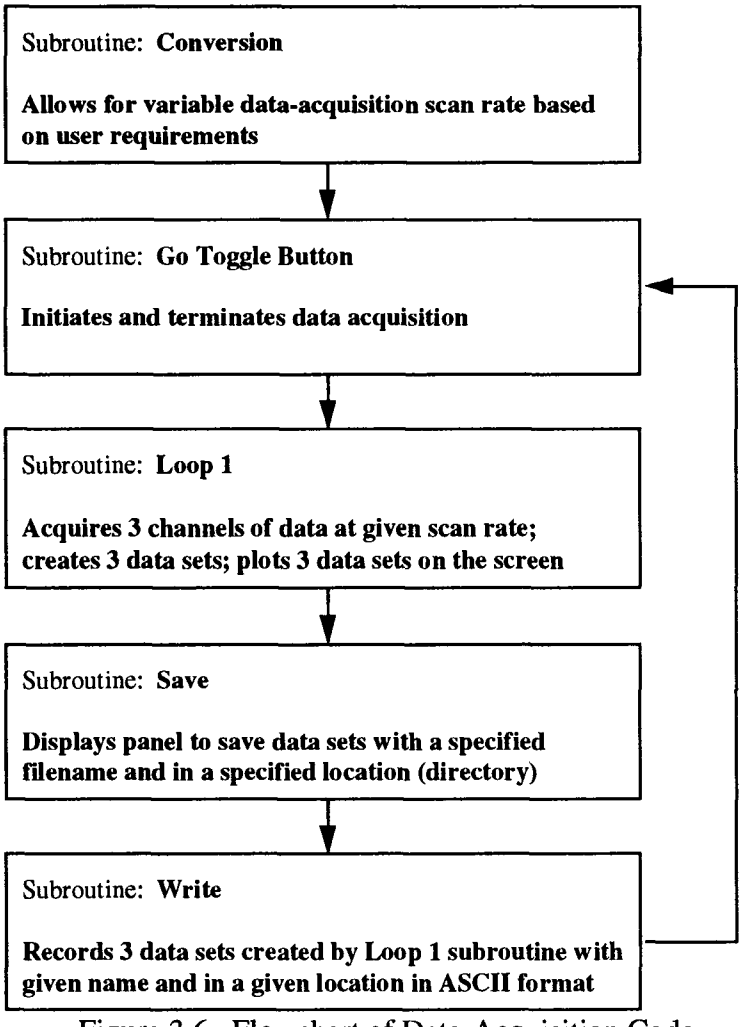

Figure 3.6. Flowchart of Data-Acquisition Code

3.6. Force Calibration

Calibration is the process of converting raw data (e.g., output voltage) into meaningful values of the appropriate unit. Figure 3.7 is a typical plot of the raw output voltage vs. grinding time in the normal-force direction for a downgrinding pass. The calibration process provides a one-to-one relationship between the raw output voltage recorded by the data-acquisition system and the forces encountered by the workpiece during the grinding process. Figure 3.8 shows a plot of the normal grinding forces calculated from the raw output-voltage data from Figure 3.7. The relationship between output voltage and grinding force obtained through the calibration process is applied before plotting Figure 3.8. Note the two units: they are voltage and Newtons respectively.

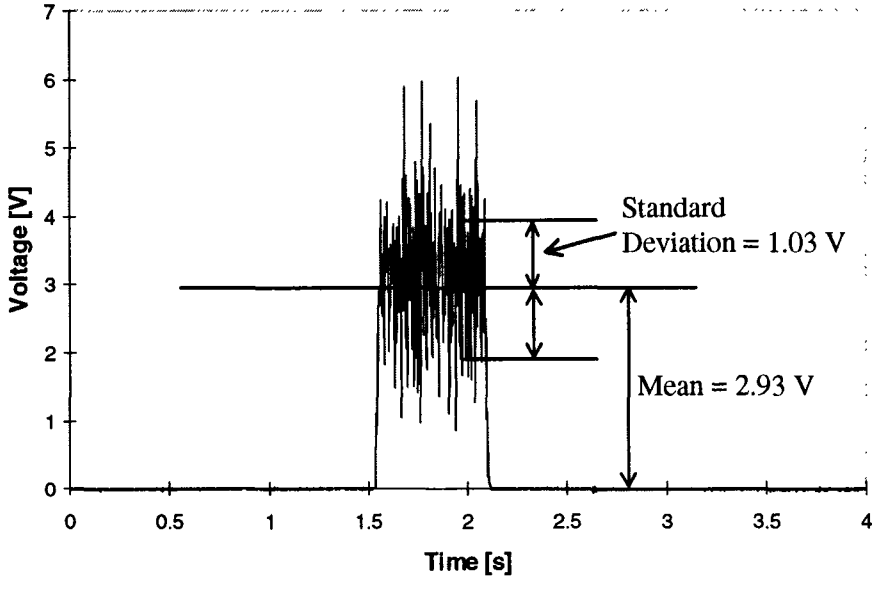

Figure 3.7. Typical Raw Output-Voltage Data From Grinding Experiment

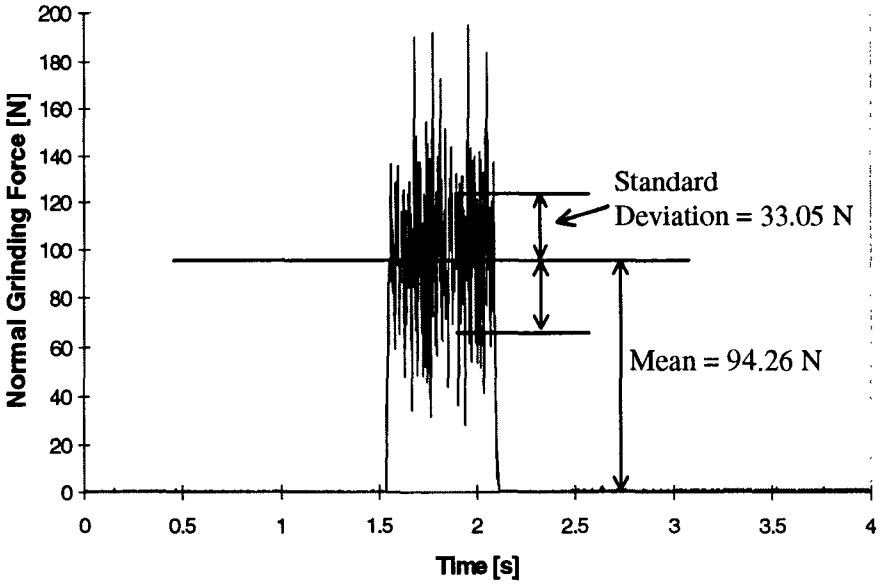

Figure 3.8 Normal Grinding Force From Calibrated Raw Voltage Data

The 3-component Kistler dynamometer should be calibrated in all three force directions (normal, tangential, and transverse) before being used to collect force data. The first step of the calibration process is to subject the dynamometer to a known set of forces (weights were used for direct calibration) in all the directions of the forces, and to record the corresponding output-voltage displacement. Figure 3.9 shows the calibration process for the dynamometer in the normal force direction. The dynamometer was calibrated in the tangential and transverse directions by using a simple pulley arrangement to apply the force to the dynamometer. "Displacement" of the output voltage refers to the difference between the baseline voltage -- before the dynamometer was subjected to the weights -- and the output voltage corresponding to the applied static force.

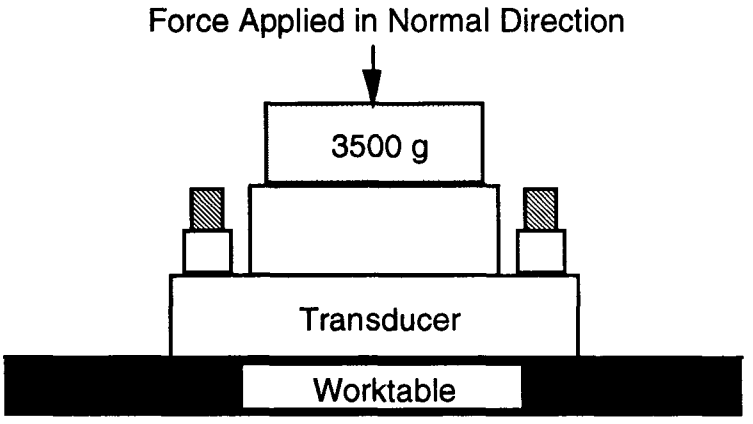

Figure 3.9. Calibration of Dynamometer in Normal Direction

The second step of the calibration process plots voltage data against force data to provide a relationship between the measured data and physical value. The transformation matrix [T] describes the relationship between the input force [F] and the output voltage [V] [Hwang 1992].

$$[V] = [T][F]$$

or

$$\begin{bmatrix} V_x \\ V_y \\ V_z \end{bmatrix} = \begin{bmatrix} \frac{\Delta V_x}{\Delta F_x} & \frac{\Delta V_x}{\Delta F_y} & \frac{\Delta V_x}{\Delta F_z} \\ \frac{\Delta V_y}{\Delta F_x} & \frac{\Delta V_y}{\Delta F_y} & \frac{\Delta V_y}{\Delta F_z} \\ \frac{\Delta V_z}{\Delta F_x} & \frac{\Delta V_z}{\Delta F_y} & \frac{\Delta V_z}{\Delta F_z} \end{bmatrix} \begin{bmatrix} F_x \\ F_y \\ F_z \end{bmatrix}$$

Multiplication of the inverse of the transformation matrix by the recorded experiment voltage values permits calculation of the grinding-force values.

$$[F] = [T]^{-1}[V]$$

Figures 3.10-3.12 are plots of voltage displacement versus the applied static load for the three separate force directions. The six off-diagonal terms of the transformation matrix are negligible, as these crosstalk terms are nearly zero. A least-squares fit through the data points results in a linear relationship between the two quantities. The equation of the best-fit lines allow transformation of the raw voltage data into grinding forces.

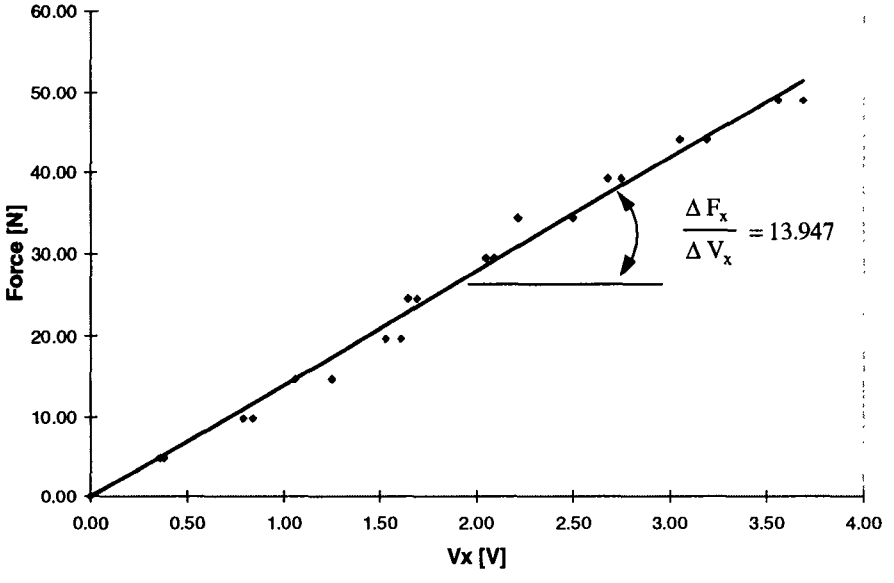

Figure 3.10. Dynamometer-Calibration Curve in Transverse Direction

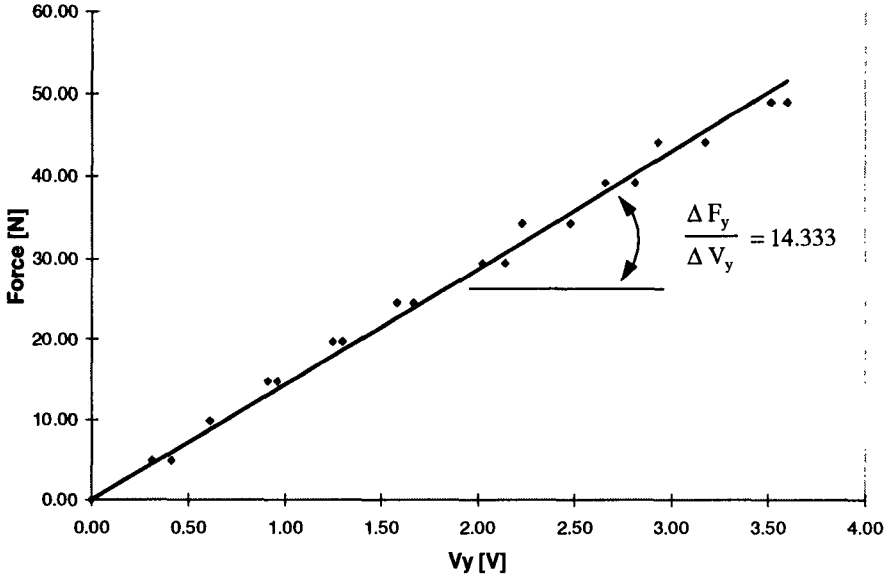

Figure 3.11. Dynamometer-Calibration Curve in Tangential Direction

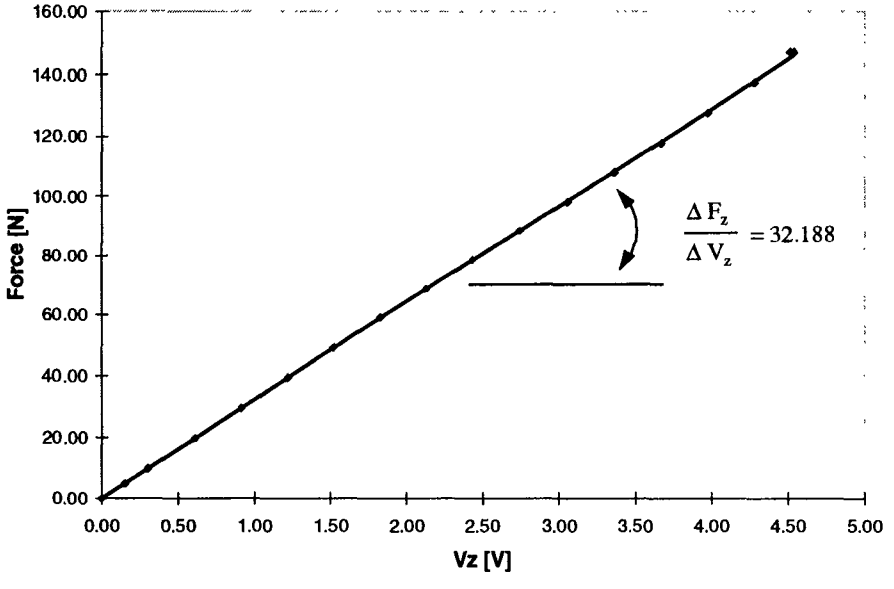

Figure 3.12. Dynamometer-Calibration Curve in Normal Direction

3.7. Wear Measurement

Wheel-wear measurements provide quantitative information on the effect of the grinding condition. Ceramic specimens, narrower than the wheel's width, were plunge-ground to produce a groove in the wheel as a result of wear. Figure 3.13 shows the plunge-grinding mode.

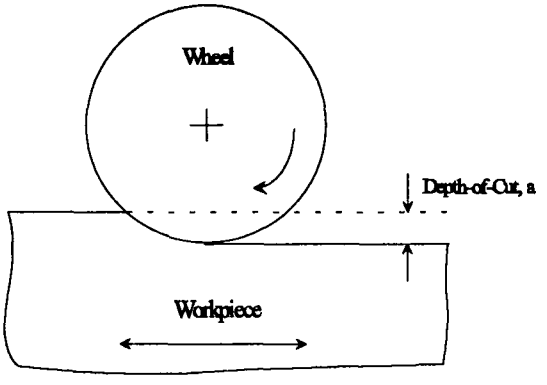

Figure 3.13. Plunge-Grinding Mode

Figure 3.14 shows the grinding wheel before and after the grinding experiments: the grinding wheel shows no wear before the grinding experiments (left figure), and a groove worn into the grinding wheel after the experiments (right figure). The depth of the wear groove provides an index to quantify the wheel wear resulting from grinding ceramic material. The width of the wear groove should equal the width of the workpiece and should remain unchanged during grinding, except for a minimal increase from interacting with the sides of the silicon nitride specimens and from abrasion caused by debris in the grinding fluid.

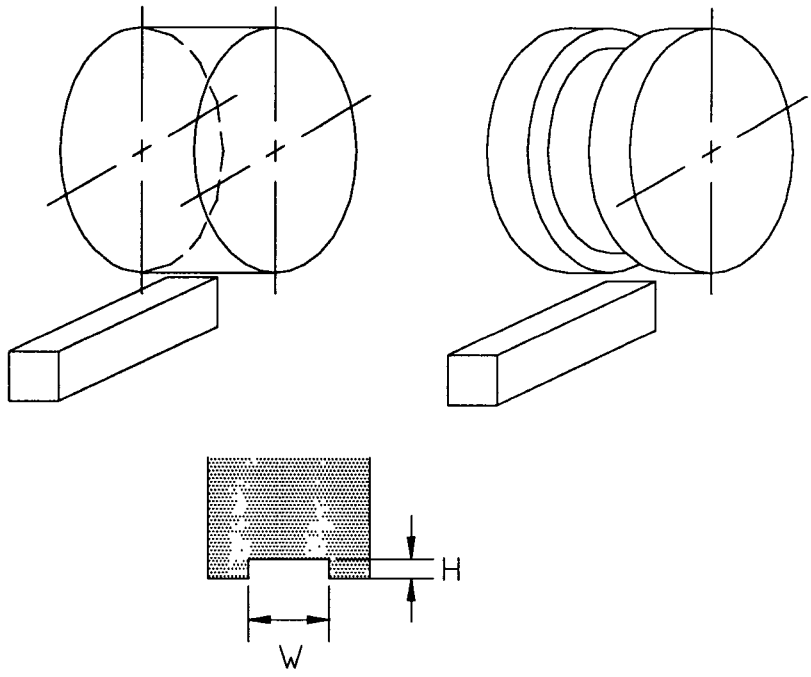

Figure 3.14. Wheel-Wear Measurement

Wheel wear can be measured by grinding a soft glass to duplicate the wear groove. Figure 3.15 shows the duplication pattern of the wear groove ground into the soft soda-lime glass specimen. Stylus-profilometry tracing across the duplication pattern of wear groove in the glass specimen allows calculation of the cross-sectional area of the wear groove; multiplying this area by the circumference of the wheel provides the volumetric wheel wear.

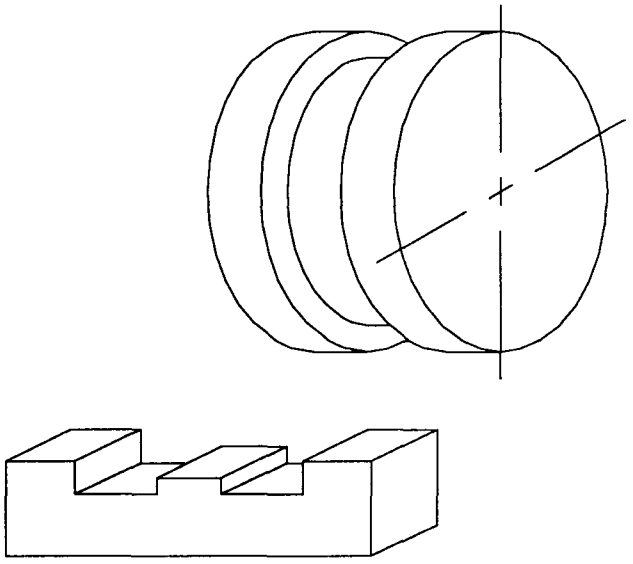

Figure 3.15. Duplication Pattern of the Wear Groove in a Soft Glass Specimen

Glass was considered the best impression material because of its low hardness and low grinding force, which would prevent additional wear to the grinding wheel during the wheel-wear measurements. Figure 3.16 shows the removable aluminum mounting plates to which the glass slides were attached: the removable design allowed the mounting plates to be detached from the steel mounting plate during the wear experiments. Several grinding profiles could be ground into the glass slide, as the width of the slide could accommodate six or seven side-by-side profiles.

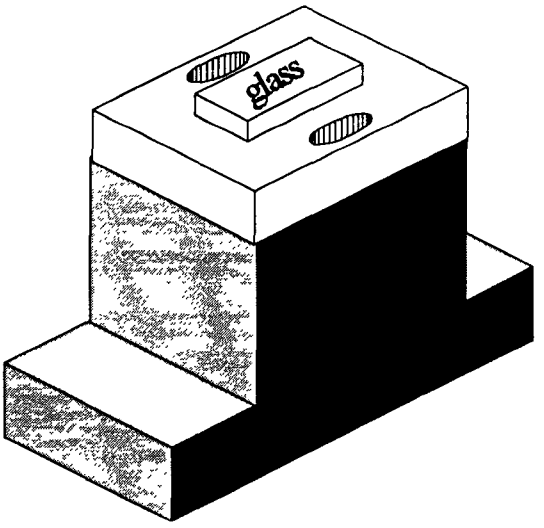

Figure 3.16. Wheel-Wear Impression Setup

The wheel-wear profiles were recorded using a Mahr-Perthen Perthometer S5p, a stylus profilometer that uses a 5 μm-radius tip stylus to physically trace across the surface and record the profile curve onto a thermal paper. The profile traces of the glass impressions were digitized by scanning using the "Un-Scan-It" software. The software converted the scanned profile images into x,y data points that were used to determine the cross-sectional wear area of the grinding groove, thus calculating the wear volume of the grinding wheel. Figures 3.17 - 3.18 are typical plots of the x,y data points produced from a scanned image of the profilometry traces of the duplication patterns of the grinding wheel before grinding, and after grinding, 4100 mm^3 of material, respectively. The area between the two curves represents the cross-sectional area of the wear groove produced during the wear experiments.

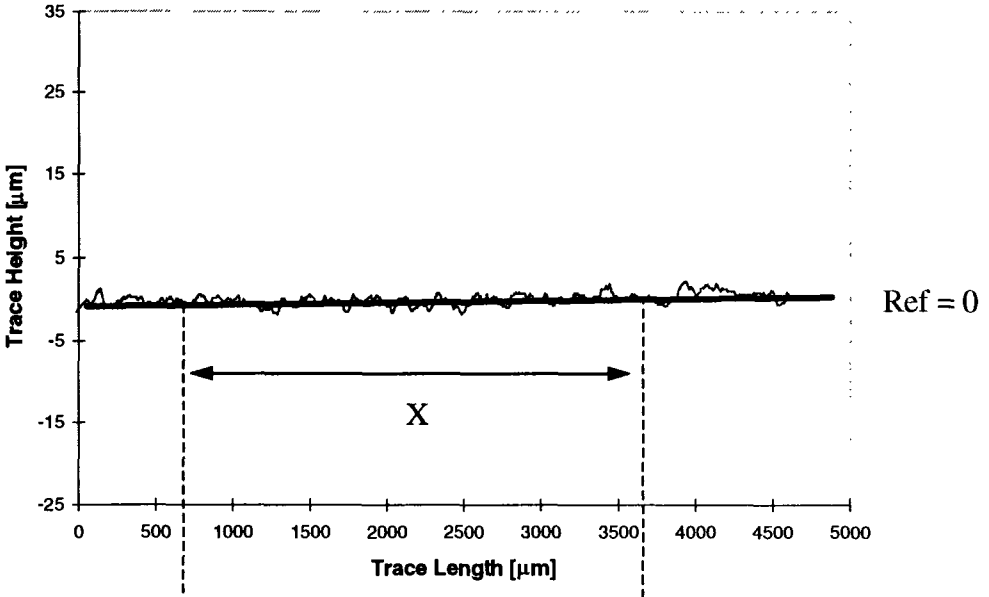

Figure 3.17. Discrete Data of the Trace of an Unworn Wheel -- Before Grinding

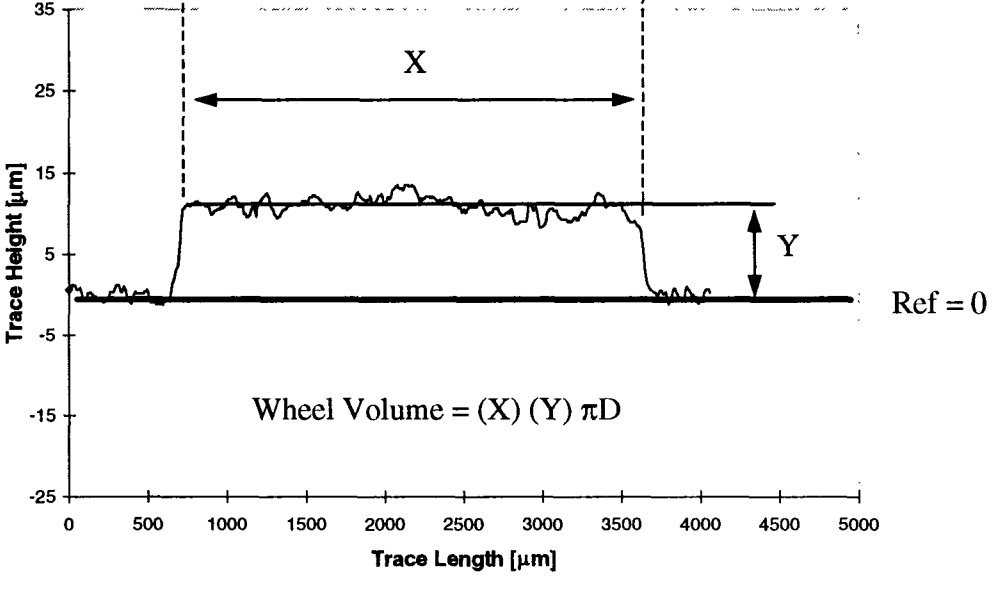

Figure 3.18. Discrete Data of the Trace of the Wear Groove -- After 4100 mm^3 Removed

3.8. Surface Roughness Measurements

Roughness measurements serve to indicate the quality of the machined surface. For this research, a Mahr-Perthen Perthometer S5p 2-dimensional stylus profilometer provided surface-roughness measurements of the ground ceramic workpieces. Plunge-grinding was performed in the longitudinal direction or along the length of the wear specimen; therefore, roughness was measured by tracing the profilometer stylus across the silicon nitride specimens perpendicular to the grinding direction (i.e., along the width of the specimen). A trace length of 1.8 mm and a cutoff length (filter) $\lambda = 0.25$ were used for the preliminary wear experiments. A trace length of 1.8 mm and a cutoff length $\lambda = 0.08$ were used for the later experiments.

3.9. Test Procedure

The grinding experiments were performed using peripheral grinding wheels mounted on a Chevalier grinder. The wheels were Cincinnati Milacron CM(*grit size*)-P100-B-1/8 resin-bonded with GE RVG-880 diamond. The test specimens were ground in the plunge-grinding mode (grinding without a crossfeed) by controlling the downfeed and table movement manually. Three sets of experiments were performed in the investigation of wheel wear and its effect on forces in grinding silicon nitride: the first experiment ground three types of silicon nitrides to investigate the magnitude of the grinding forces generated during grinding. The second experiment was a preliminary wear test to compare the wear of SSN and SRBSN on the diamond grinding wheel.

These preliminary wear experiments also served to establish and refine a test procedure for the subsequent extended wheel-wear experiments using SRBSN. The third experiment was a wear experiment using SRBSN to investigate the effect of machining condition: i.e., downfeed on the wheel wear of the grinding wheel. The following is a detailed description of the three experiments.

Before the wheel-wear experiments began, several grinding tests were conducted to compare the normal- and tangential-force magnitudes of three silicon nitride ceramics: reaction-bonded silicon nitride (RBSN), sintered silicon nitride (SSN), and sintered reaction-bonded silicon nitride (SRBSN). The three silicon nitride materials were mounted in two rows, randomizing the specimens in each row, and ground under various conditions. The force experiments used an 8-inch, 80-grit (Cincinnati Milacron CMD80-P100-B-1/8) diamond wheel. The downfeeds were set at 50 μm per pass and 125 μm per pass; the table speed was set at 0.125 m/s; and the wheel speed was fixed at 3600 RPM (approximately 38 m/s).

The SSN and SRBSN preliminary wear experiments used an 8-inch, 80- and 150-grit diamond wheel, respectively, to establish the wheel-wear procedure and to investigate the sensitivity of the wheel-wear measurements. The SSN specimens were mounted in two rows of three samples per row and the SRBSN specimens were mounted in six rows of two samples per row. The downfeed was set at 50 μm per pass; the table speed was set at 0.125 m/s; and the wheel speed was fixed at 3600 RPM (approximately 38 m/s). Wear and force measurements were performed using alternate upgrinding and

downgrinding passes across the ceramic specimens. Upgrinding and downgrinding are the motions of the workpiece relative to the rotational direction of the grinding wheel: i.e., clockwise or counterclockwise. Figure 3.19 shows the upgrinding (left figure) and downgrinding (right figure) process.

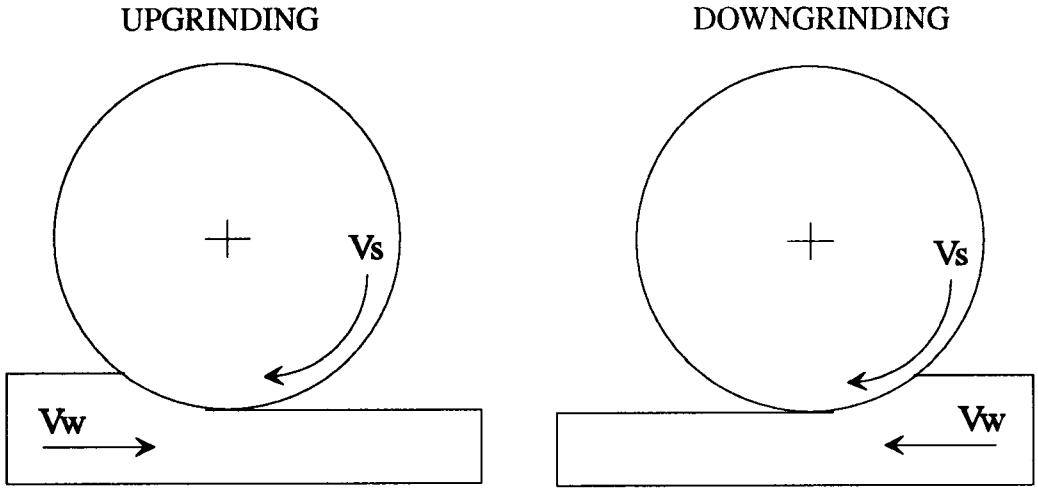

Figure 3.19. Upgrinding and Downgrinding Processes

The specific material removal rate Q'_w (defined as $Q'_w = v/d$ where v is the table speed and d is the downfeed) for the SSN and SRBSN wear experiments was $Q'_w = 6.25\ mm^3/(mm \cdot s)$. The grit depth-of-cuts h_{max} were $h_{max} = 1.48\ \mu m$ and $h_{max} = 0.82\ \mu m$, respectively. The volume of material ground during these experiments (V) is defined as V = number of grinding passes x width of specimen x length of specimen x downfeed. A total 140 passes, equaling a volume of 3150 mm^3 of SSN (140 x 3mm x 150mm x 0.05mm = 3150 mm^3), was ground, as well as a total 420 passes, equaling a volume of 6300 mm^3 of SRBSN (420 x 3mm x 100mm x 0.05mm = 6300 mm^3). Grinding-wheel profiles were ground into the glass specimens at intervals after the diamond-grit grinding

wheel removed approximately 500 mm^3 of SSN and after approximately 1000 mm^3 of SRBSN.

The final set of wear tests was conducted to investigate the effect of machining condition: i.e., increased downfeed on the wheel wear of the grinding wheel. These experiments were performed using SRBSN and holding all variables constant except for downfeed. For these experiments, six times the previous volume of SRBSN was ground using the same 6-inch, 150-grit (Cincinnati Milacron CMD150-P100-B-1/8) diamond grinding wheel. The specimens for these experiments were mounted with one sample in each row. The table speed was set at 0.125 m/s and the wheel speed maintained at 30 m/s. The first experiment used a downfeed set at 50 μm per pass for a total 2890 passes, equaling a volume of 35918 mm^3 of SRBSN; in the second experiment, the downfeed was increased to 125 μm per pass for a total 1284 passes equaling a volume of 37910 mm^3 of SRBSN. The corresponding specific material-removal rates (Q'_w for the first and second experiments) were Q'_w = 6.25 $mm^3/(mm \cdot s)$ and Q'_w = 15.625 $mm^3/mm \cdot s$, respectively. The corresponding grit depth-of-cuts for the two experiments were h_{max} = 0.99 μm and h_{max} = 1.25 μm respectively. In the first experiment, grinding-wheel profiles were ground into the glass specimens at intervals after approximately 5000 mm^3 of SRBSN was removed by the diamond-grit grinding wheel. In the second experiment, grinding-wheel profiles were ground into silicon nitride at intervals after approximately 5000 mm^3 of SRBSN was removed by the diamond-grit grinding wheel. The change

from glass to silicon nitride was made because SRBSN material was easier to prepare and there was no change in the wear results.

Chapter 4

Results

4.1. Preliminary Force Measurements

Preliminary grinding-force measurements of sintered silicon nitride (SSN), reaction-bonded silicon nitride (RBSN), and sintered reaction-bonded silicon nitride (SRBSN) were made to provide grinding-force information for use in planning the subsequent wear experiments. Figures 4.1, 4.2, and 4.3 are representative plots of the normal, tangential, and transverse grinding forces respectively for the three silicon nitride materials ground using an 80-grit wheel, the downfeed set at 125-μm; the table speed set at 0.125 m/s; and the wheel speed fixed at 3600 RPM (approximately 38 m/s). In general, grinding forces for the RBSN material were the lowest of the three silicon nitride ceramics and grinding forces for the SRBSN material were the highest; however, grinding forces for the SSN material were not significantly less than those for SRBSN. Differences in grinding forces among the three ceramics are related to the mechanical properties of the three materials. The large variation in grinding forces can be attributed to the resonance frequency of the dynamometer matching that of the grinding process. Table 4.1 sets forth the normal, tangential, and transverse grinding forces, standard deviations, and the measured table speed for a series of nine repeated grinding experiments for these three materials. The grinding conditions for the nine repeated experiments were: an 80-grit wheel; the downfeed was set at 50-μm per pass; the table speed was set at 0.125 m/s; and the wheel speed was fixed at 3600 RPM (approximately

38 m/s). The table demonstrates the changes in grinding forces and standard deviations between experiments for similar grinding conditions.

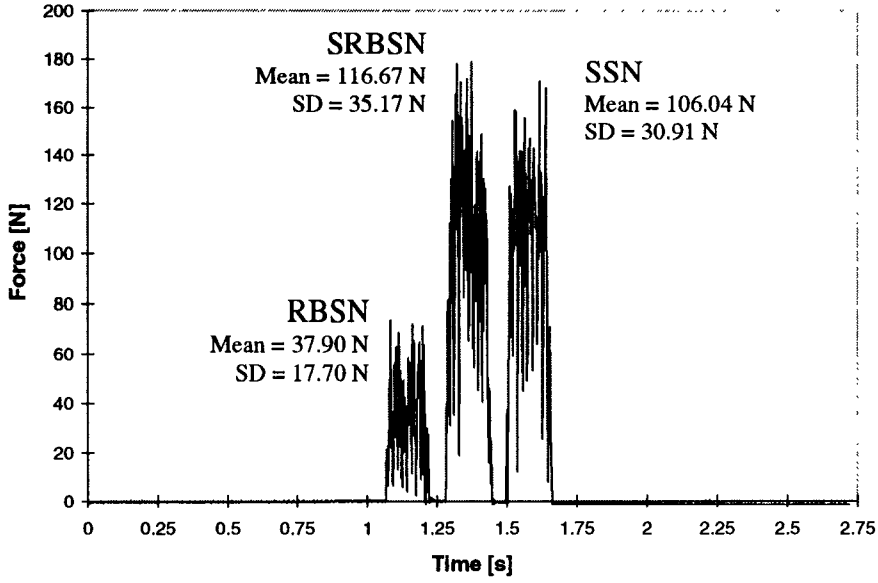

Figure 4.1. Normal Grinding Forces of RBSN, SRBSN, & SSN Silicon Nitrides

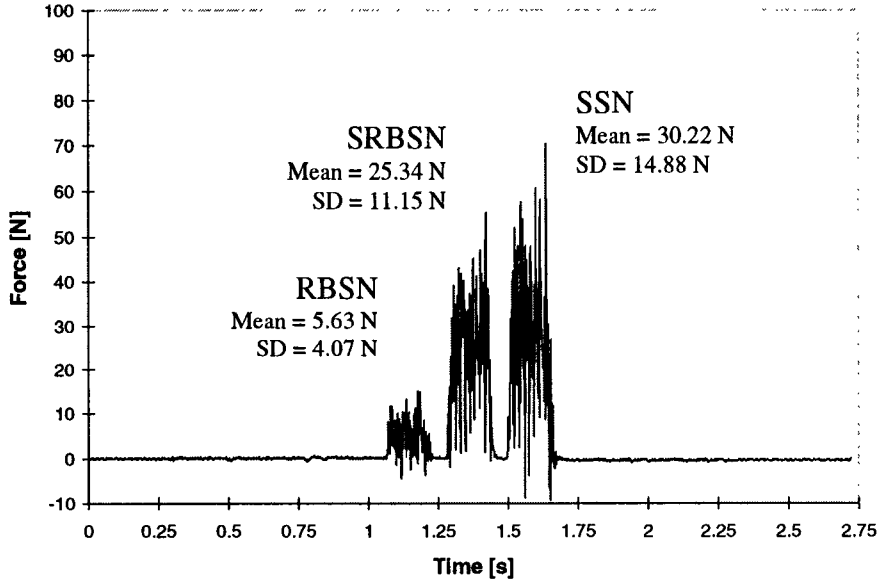

Figure 4.2. Tangential Grinding Forces of RBSN, SRBSN, & SSN Silicon Nitrides

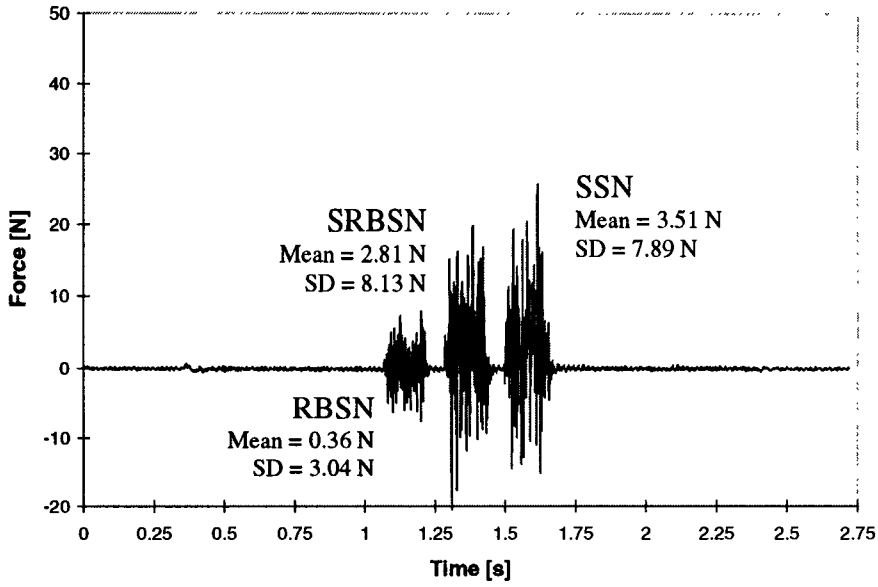

Figure 4.3. Transverse Grinding Forces of RBSN, SRBSN, & SSN Silicon Nitrides

Table 4.1. Grinding Forces for SSN, RBSN, and SRBSN

Material	Direction	Experiment 1			Experiment 2			Experiment 3		
		Force [N]	Standard Deviation	Vw [mm/s]	Force [N]	Standard Deviation	Vw [mm/s]	Force [N]	Standard Deviation	Vw [mm/s]
	Transverse	0.46	11.92		0.23	12.02		0.43	12.18	
RBSN	Tangential	1.94	2.03	13.42	1.57	1.62	16.11	1.76	1.68	12 72
	Normal	16.32	18.47		15.47	19.17		14.17	15.63	
	Transverse	0.55	11.98		0.82	12.44		1.30	12.82	
SRBSN	Tangential	8.18	8.62	13.80	7.40	7.45	16.10	7.85	7.78	13.80
	Normal	39.98	41.78		38.44	41.99		42.36	43.78	
	Transverse	0.82	12.14		1.42	12.90		1.08	12.66	
SSN	Tangential	7.75	7.98	12.76	7 48	7.53	13.85	6.43	6.35	12.12
	Normal	36.82	39.61		43.03	46.57		37.13	38.55	
Material	Direction	Experiment 4			Experiment 5			Experiment 6		
		Force [N]	Standard Deviation	Vw [mm/s]	Force [N]	Standard Deviation	Vw [mm/s]	Force [N]	Standard Deviation	Vw [mm/s]
	Transverse	0.30	12.22		0.21	11.85		0.43	12.00	
RBSN	Tangential	1.48	1.44	13.81	1.58	1.55	13.81	1.58	1.68	13 81
	Normal	14.55	17.57		15.23	14.71		13.20	14.64	
	Transverse	1.25	12.91		1.57	12 84		1.69	12.94	
SRBSN	Tangential	7.75	7.71	13.80	7 79	7.76	13.80	6.93	7.03	13.80
	Normal	35.47	38.36		45.03	44.48		43.42	44.82	
	Transverse	1.54	13.13		1.61	12.86		1 81	13.03	
SSN	Tangential	7.27	7.23	12.76	6.52	6.48	13.85	6.12	6.21	13.85
	Normal	40.67	43.56		31.91	40.45		37.37	38.77	
Material	Direction	Experiment 7			Experiment 8			Experiment 9		
		Force [N]	Standard Deviation	Vw [mm/s]	Force [N]	Standard Deviation	Vw [mm/s]	Force [N]	Standard Deviation	Vw [mm/s]
	Transverse	0.40	12.13		0.37	11 54		0.33	11.73	
RBSN	Tangential	1.72	1.78	16.11	1.68	1.74	13.81	1.45	1.56	13.81
	Normal	15.88	18.06		13.45	14.71		14.72	14.60	
	Transverse	1.30	12.80		1.65	11.99		1.44	12.56	
SRBSN	Tangential	6.57	6.63	13.80	6.67	6.44	13.80	7.55	7.66	13.80
	Normal	44.02	46.13		44.34	37.41		49 09	48.97	
	Transverse	1.09	12.64		1.78	11.74		1.44	12.56	
SSN	Tangential	6.32	6.37	13.85	6.23	5.22	13.85	7.34	7.45	13.85
	Normal	33.41	35.53		37.64	36.44		41.36	41.24	

4.2. Grinding-Force and Wheel-Wear Measurements with SSN

Figure 4.4 is a plot of the normal and tangential grinding forces vs. the volume of removed sintered silicon nitride (SSN) material. For these experiments, no distinction was made between the downgrinding and upgrinding forces. Plots of the grinding forces show the average force values obtained for one pass of the grinding wheel across the length of the specimen. The normal grinding force increased continuously from 49.7 N to 63.8 N during these tests; the normal force increased with increasing wheel wear. The tangential grinding forces increased from 13.4 N to 20.4 N. Figure 4.5 is a plot of the grinding-force ratio F_T/F_N vs. the volume of removed SSN material. The tangential forces are approximately 25 % that of the normal forces when grinding SSN, and increase slightly with increasing wheel wear. The linear-regression fit through the grinding-force ratio data was quite poor because the sampling scheme for these force measurements did not account for a significant difference in upgrinding and downgrinding forces.

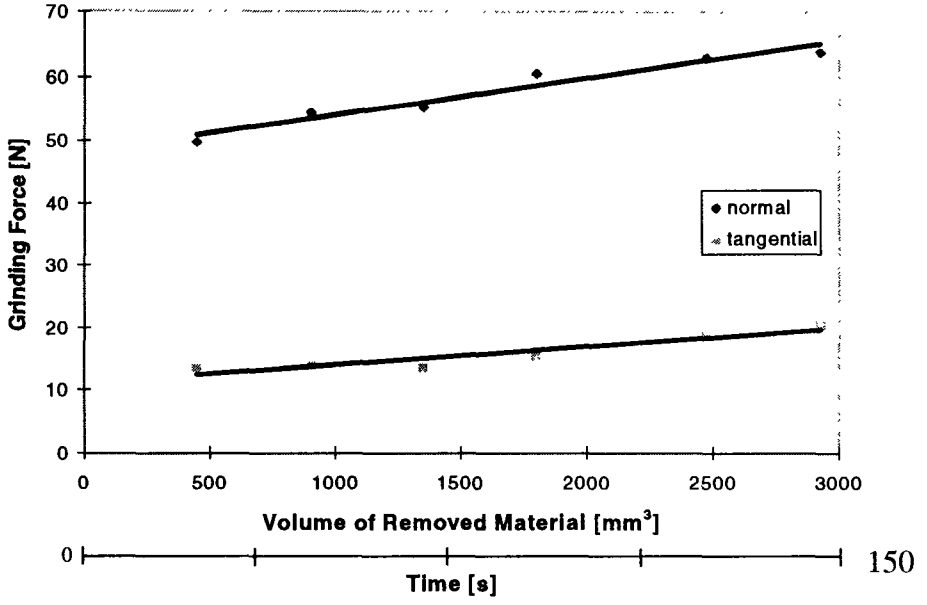

Figure 4.4. Grinding Forces for SSN

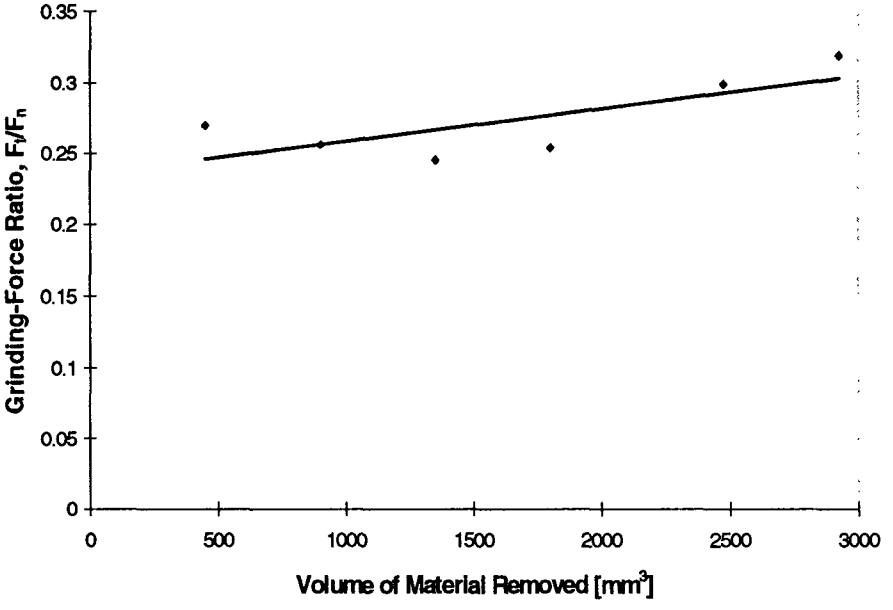

Figure 4.5. Grinding-Force Ratio for SSN

Figure 4.6 is a plot of wheel wear vs. the volume of removed SSN material. The plot shows that a large increase in wheel wear occurs within the first 500 mm^3 of ground SSN material. Wheel wear steadily increases until it ends at a wear volume of 23.7 mm^3

for 3150 mm^3 of ground SSN. Figure 4.7 is a plot of the G-ratio vs. the volume of removed SSN material. The G-ratio for this experiment quickly rises to 60 and increases gradually until ending at 130.

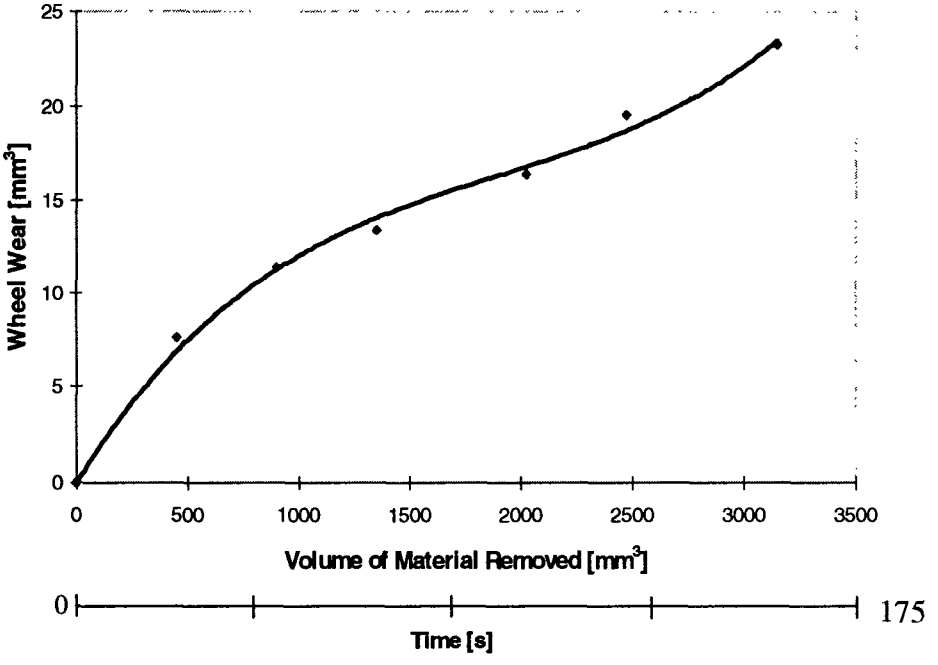

Figure 4.6. Wheel Wear for SSN

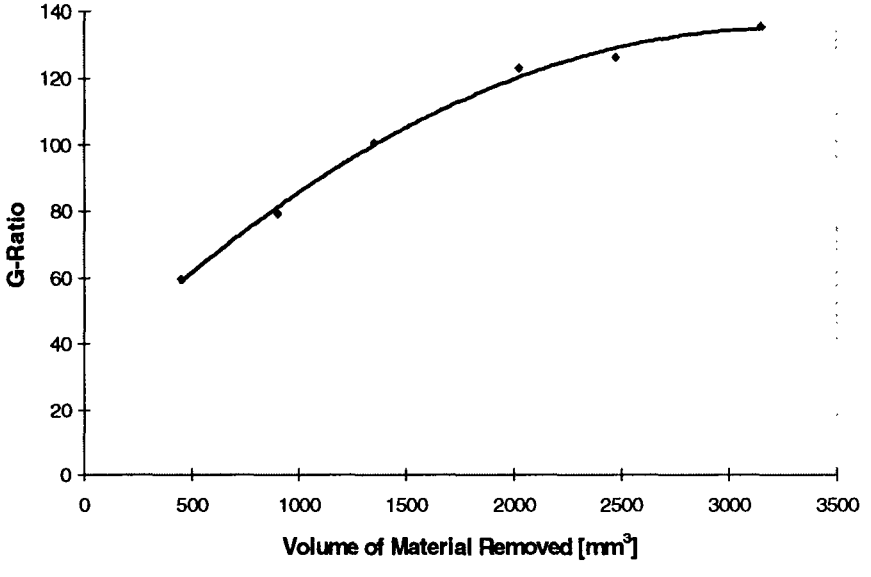

Figure 4.7. G-Ratio for SSN

Figure 4.8 is a plot of surface roughness vs. volume of removed SSN material. Surface-roughness measurements were made using a 5 μm-radius stylus. Surface roughness R_a of SSN increased from 0.75 μm to 0.89 μm for increasing wheel wear. This difference indicates that there is no significant change in the surface roughness for this experiment.

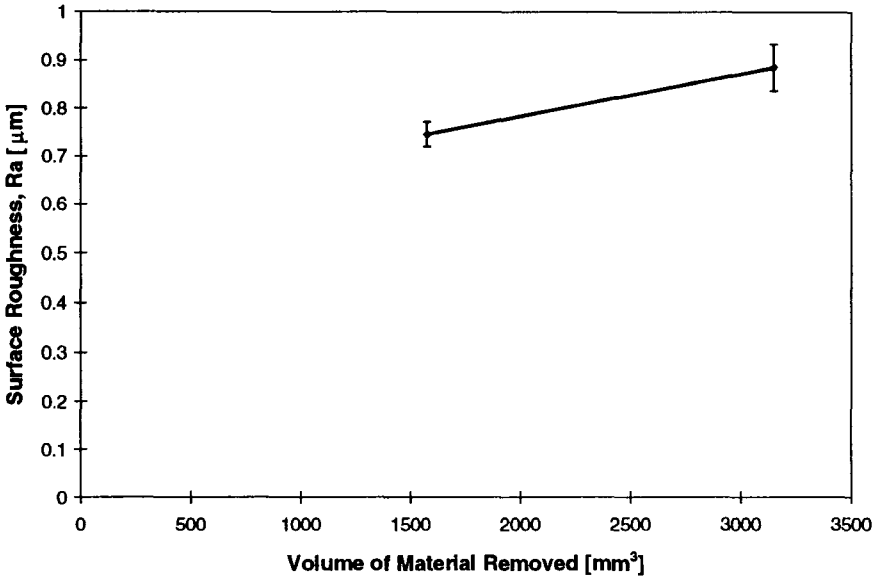

Figure 4.8. Surface Roughness for SSN

4.3. Grinding-Force and Wheel-Wear Measurements with SRBSN

Figure 4.9 is a plot of the normal and tangential downgrinding forces vs. the volume of removed SRBSN material. The normal grinding force increased steadily during these tests. Normal force increases with increasing wheel wear; the increase in

tangential grinding forces is significantly less than that during the SSN wear experiment. Figure 4.10 is a plot of the grinding-force ratio F_T/F_N vs. the volume of removed SRBSN material. The significant increase in normal grinding forces is the main factor in the decrease in grinding-force ratio. The grinding-force ratio decreases with increasing wheel wear from 0.32 to 0.22.

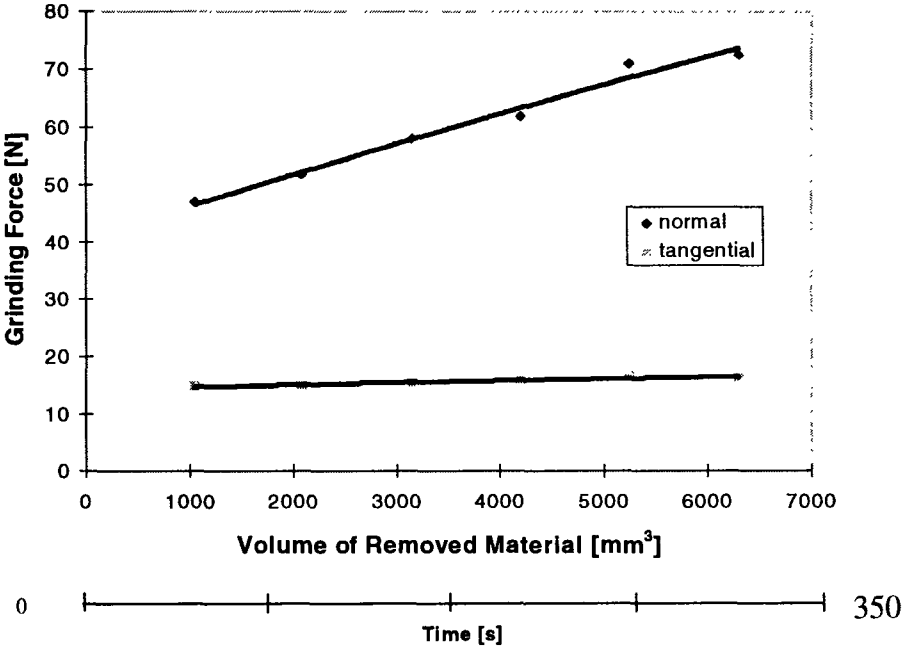

Figure 4.9. Downgrinding Forces for SRBSN

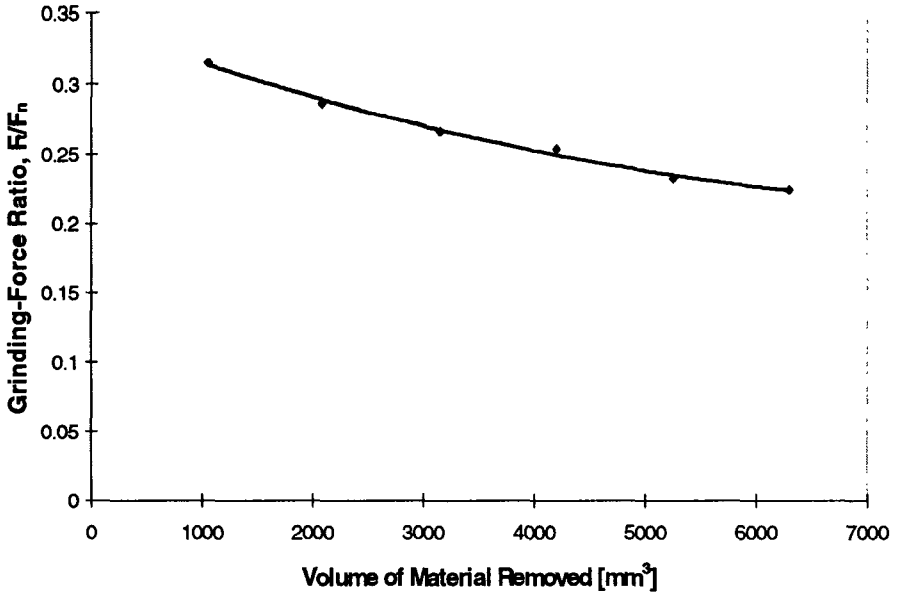

Figure 4.10. Downgrinding-Force Ratio for SRBSN

As in the SSN wear experiment, the greatest increase in wheel wear occurred during the grinding of initial 1000 mm^3 of material. Figure 4.11 is a plot of wheel wear vs. the volume of removed SRBSN material. The rapid initial wear of 11 mm^3 changed to a more gradual upward trend until it ended at a total wear volume of 17 mm^3 at 6300 mm^3 of ground SRBSN.

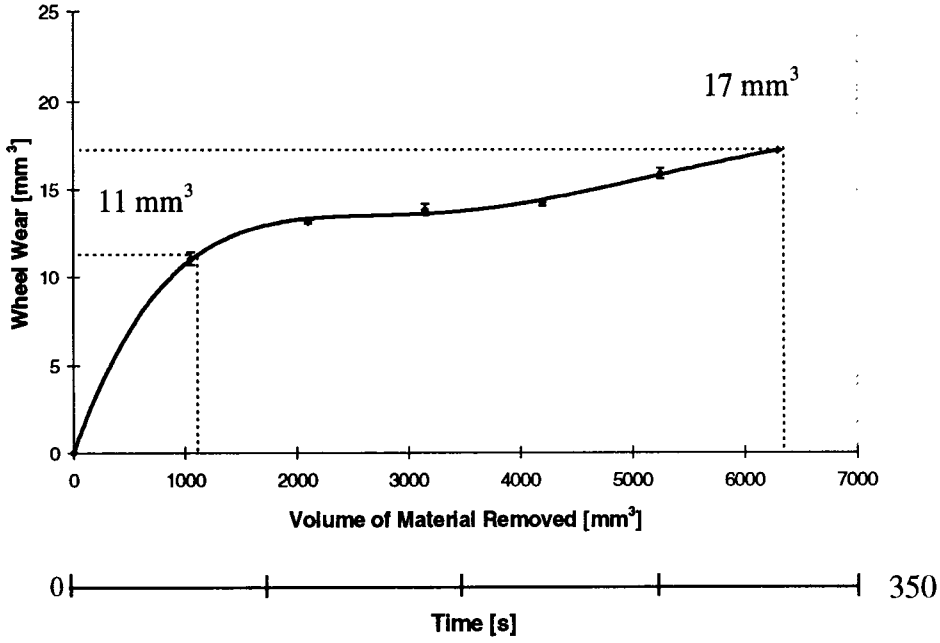

Figure 4.11. Wheel Wear for SRBSN

Figure 4.12 is a plot of the G-ratio vs. the volume of removed SRBSN material. The G-ratio after the initial 1000 mm^3 of ground SRBSN material is 100. The G-ratio increases steadily during the experiment, ending at 350. The G-ratio for SRBSN is higher than that of SSN which indicates that a greater amount of SRBSN can be removed for the same volume of wheel wear. The higher G-ratio for SRBSN suggests that the grinding wheel is better suited for grinding this material.

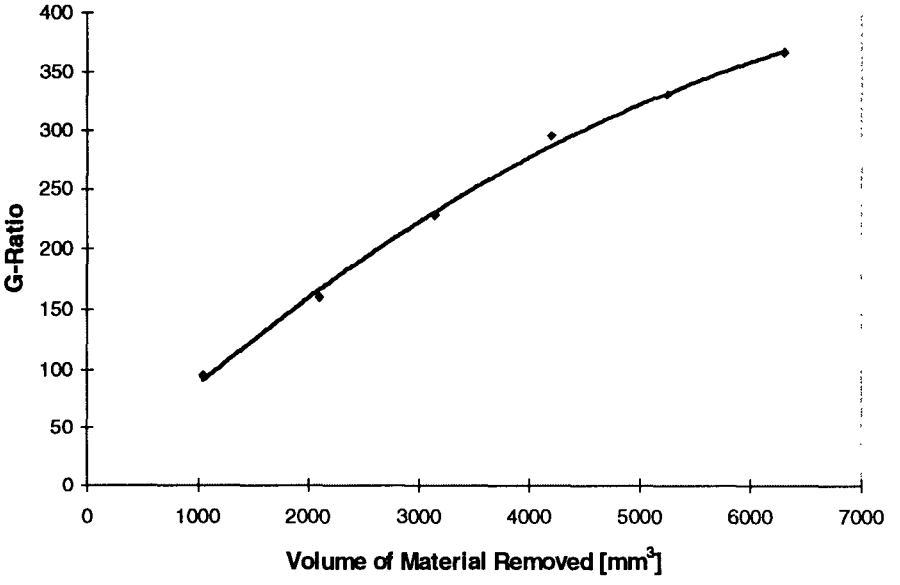

Figure 4.12. G-Ratio for SRBSN

Figure 4.13 is a plot of surface roughness vs. the volume of removed SRBSN material. Surface roughness R_a of SRBSN increased from 0.84 μm to 1.00 μm for increasing wheel wear. This change in surface roughness is not statistically significant.

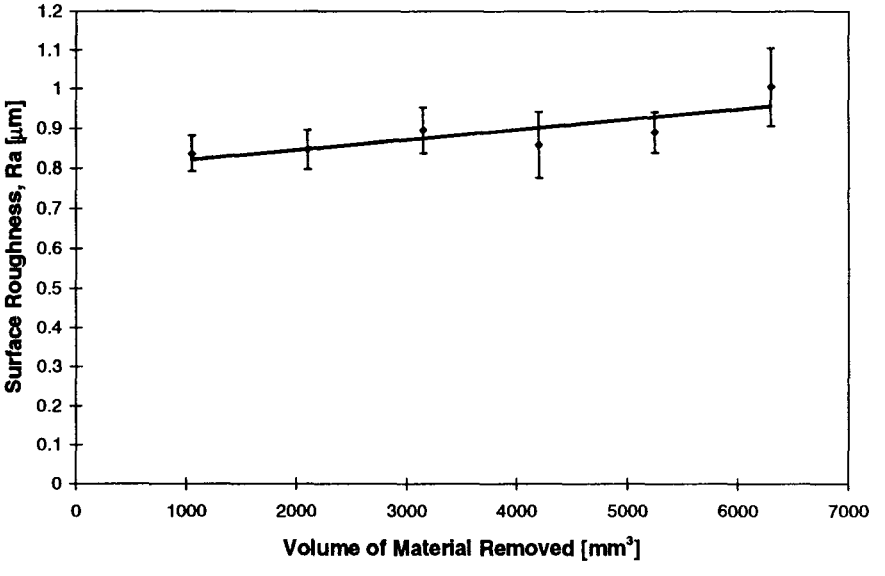

Figure 4.13. Surface Roughness for SRBSN

4.4. Effect of Grinding Condition on Wheel Wear and Grinding Forces

To further explore the accelerated wear process, extended wear tests were conducted to demonstrate whether the accelerated wear stage can be better observed by grinding a significantly greater amount of material, and to investigate the effects of grinding conditions, using the same grinding wheels, table speed, and wheel speed. The effect of grinding condition was studied by increasing the downfeed from 50 μm to 125 μm.

4.4.1. Small Downfeed

Figures 4.14-4.17 show the grinding forces and grinding-force ratios F_T/F_N for the upgrinding and downgrinding modes separately when grinding sintered reaction-bonded silicon nitride (SRBSN) at a small downfeed of 50 μm. Grinding forces and grinding-force ratios encountered in this experiment resemble those of the first SRBSN wheel-wear experiment, in comparison to the first 6300 mm^3 of removed material. The downgrinding normal grinding force increases continuously from 40 N to 130 N with increasing wheel wear; downgrinding tangential grinding force increases from 20 N to 30 N. The upgrinding grinding-force ratios range from 0.25 to 0.49, and the downgrinding grinding-force ratios range from 0.21 to 0.43. These grinding-force ratios are comparable to those for the preliminary wear experiments. Appendix C contains the

grinding-force data and standard deviations for the upgrinding process in the normal, tangential, and transverse directions.

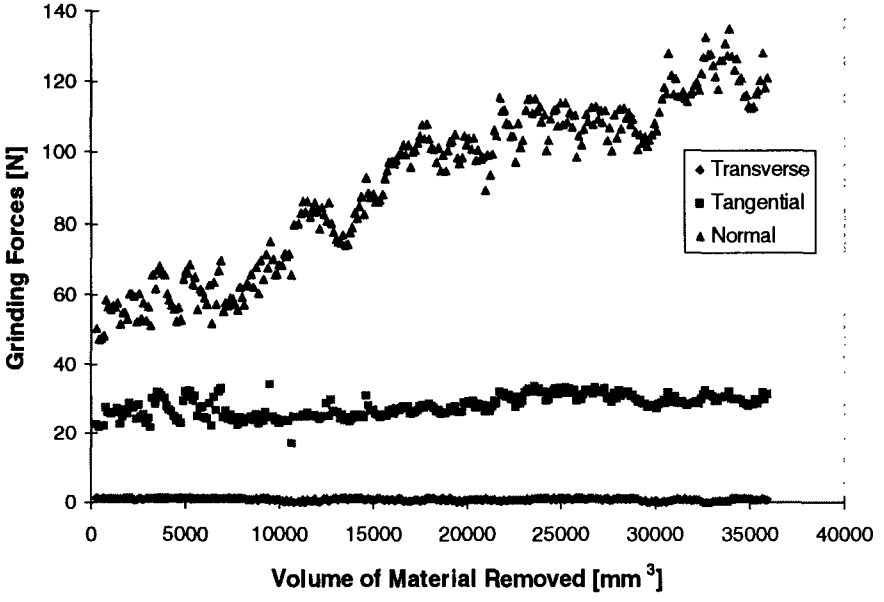

Figure 4.14. Grinding Force (Upgrinding) for SRBSN -- Small Downfeed

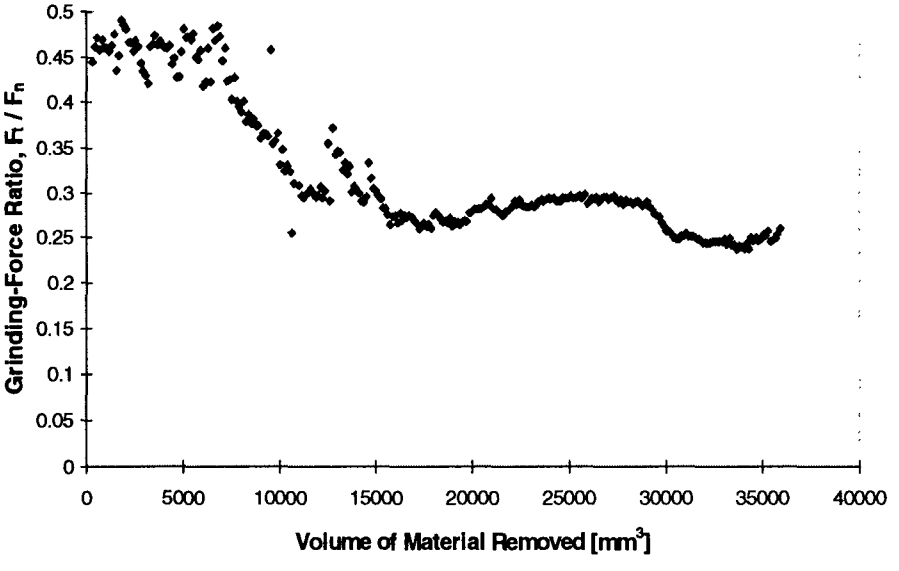

Figure 4.15. Grinding-Force Ratio (Upgrinding) for SRBSN -- Small Downfeed

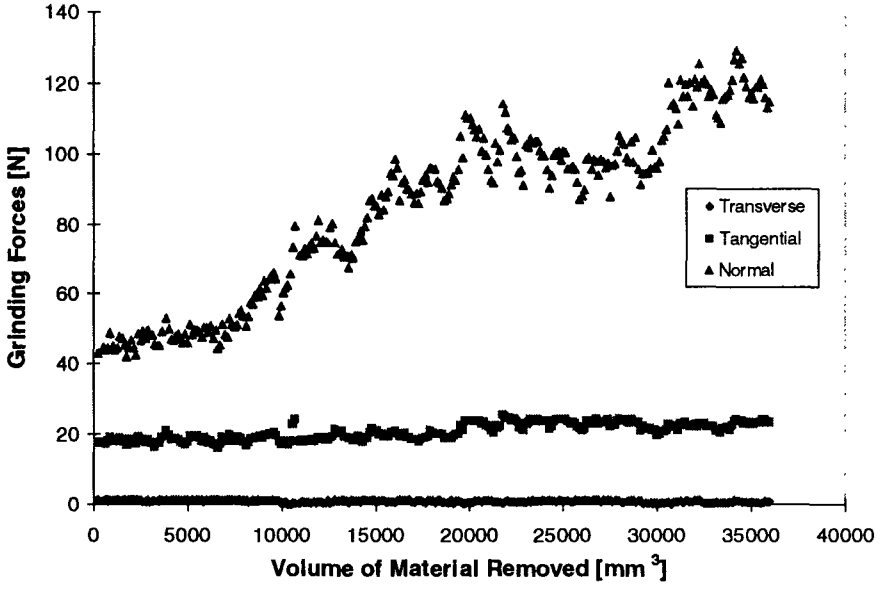

Figure 4.16. Grinding Force (Downgrinding) for SRBSN -- Small Downfeed

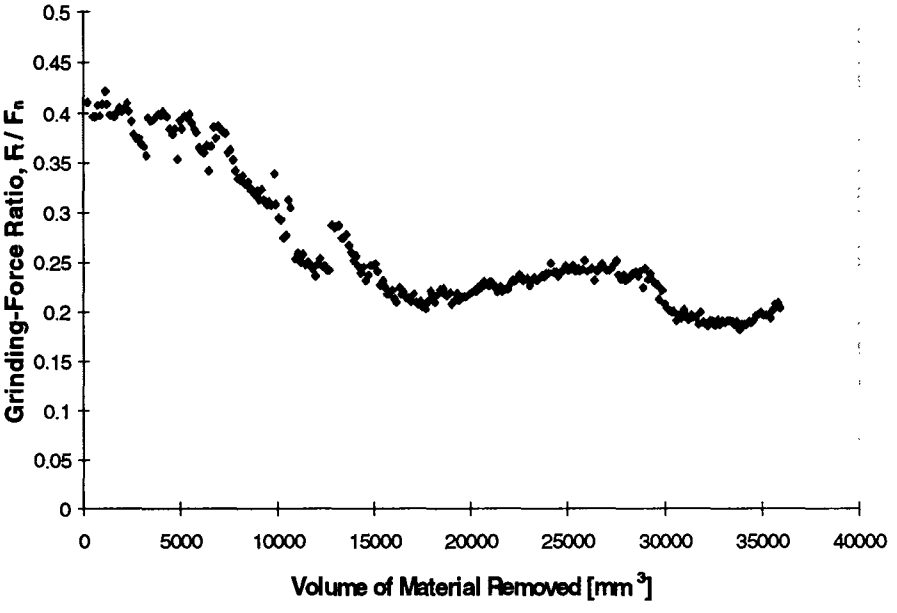

Figure 4.17. Grinding-Force Ratio (Downgrinding) for SRBSN -- Small Downfeed

Figure 4.18 is a plot of wheel wear vs. volume of removed material when grinding at a downfeed of 50 μm. Initial wear occurs between 0 and 25000 mm^3 of removed SRBSN, and normal wear progresses from 25000 mm^3 of removed SRBSN.

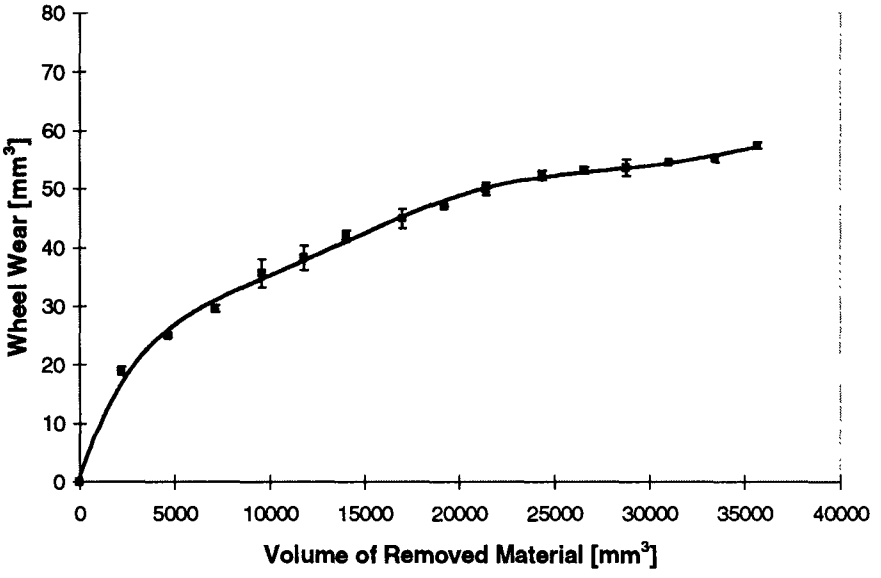

Figure 4.18. Wheel Wear vs. Material Removed for SRBSN -- Small Downfeed

Figure 4.19 is a plot of the G-ratio vs. the volume of removed SRBSN material. The G-ratio for this experiment rises sharply to 200 and continues steadily to 600 until ending around 650.

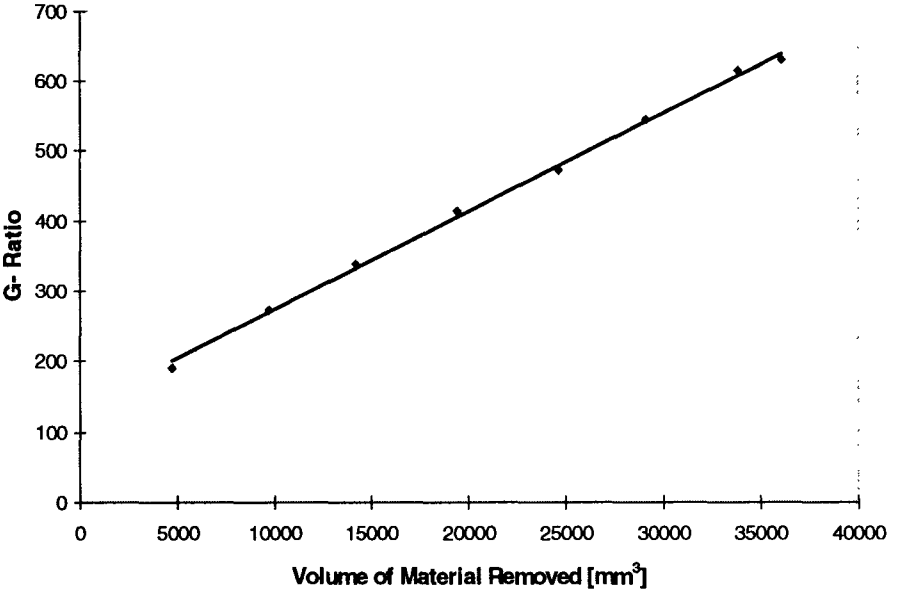

Figure 4.19. G-Ratio for SRBSN -- Small Downfeed

Figure 4.20 is a plot of surface roughness vs. volume of removed SRBSN material. Surface-roughness measurements were made using a 5 μm-radius stylus. Surface roughness follows a slightly decreasing trend. Surface roughness R_a of the SRBSN ranges from 0.42 to 0.57. These surface roughness values are lower than those recorded during the preliminary experiments because of the change in cutoff length (filter) from $\lambda = 0.25$ to $\lambda = .08$.

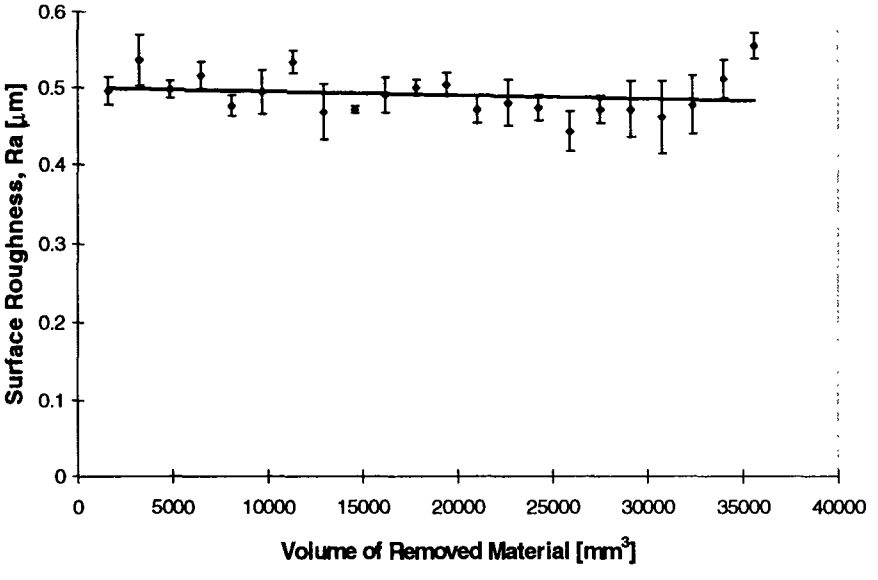

Figure 4.20. Surface Roughness for SRBSN -- Small Downfeed

4.4.2. Large Downfeed

Figures 4.21 and 4.22 show the grinding forces and grinding-force ratios for the downgrinding process, respectively, when grinding sintered reaction-bonded silicon nitride (SRBSN) at a large downfeed of 125 μm. The initial normal grinding force is three times greater than that of the previous experiment at a smaller downfeed; however,

there is no significant increase in force throughout the experiment. The variation in the normal grinding forces for the smaller downfeed experiment is typical when grinding a large volume of material [Tricard 1995]. The variation in forces most probably results from the diamond particles, becoming dull and subsequently replaced as new diamond particles become exposed from the bond; therefore, if more frequent exposure of fresh diamond particles occurs during the severe grinding condition, the variation in force should drop as the results indicate. The tangential grinding force begins twice as high as in the experiment at the 50 μm downfeed, and follows a similar trend. The grinding-force ratio decreases slightly from 0.37 to 0.33.

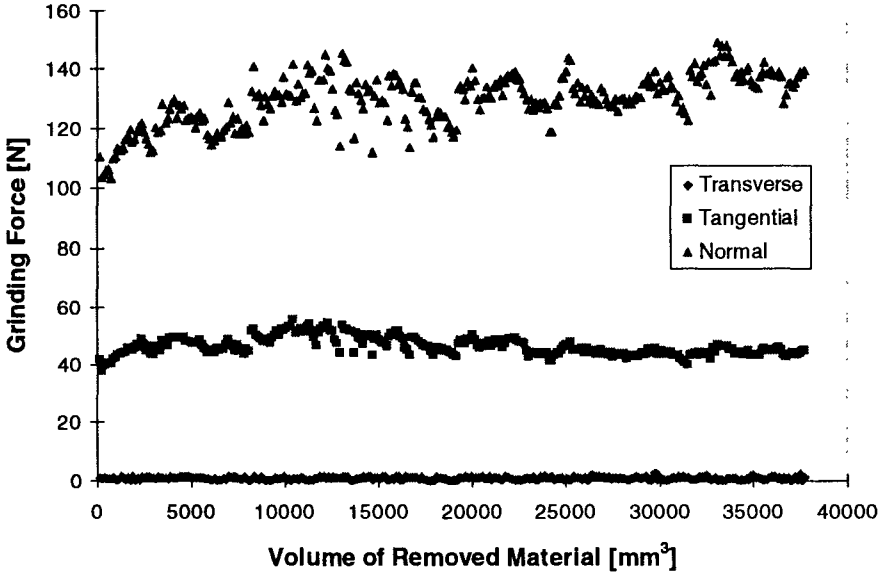

Figure 4.21. Grinding Force (Downgrinding) for SRBSN -- Large Downfeed

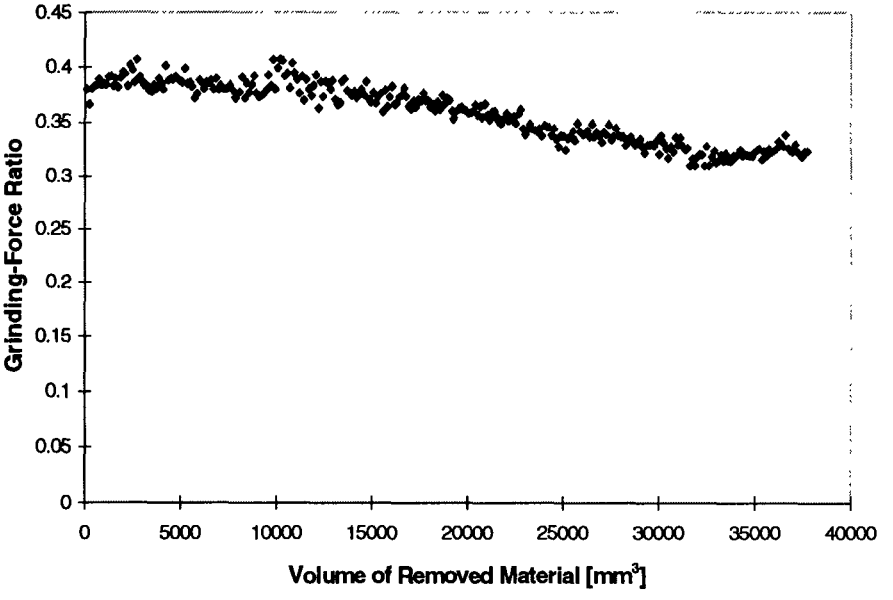

Figure 4.22. Grinding-Force Ratio (Downgrinding) for SRBSN -- Large Downfeed

Figure 4.23 is a plot of wheel wear vs. volume of removed SRBSN using the same scale of the small-downfeed plot. As expected, the more severe grinding condition causes greater wear of the grinding wheel.

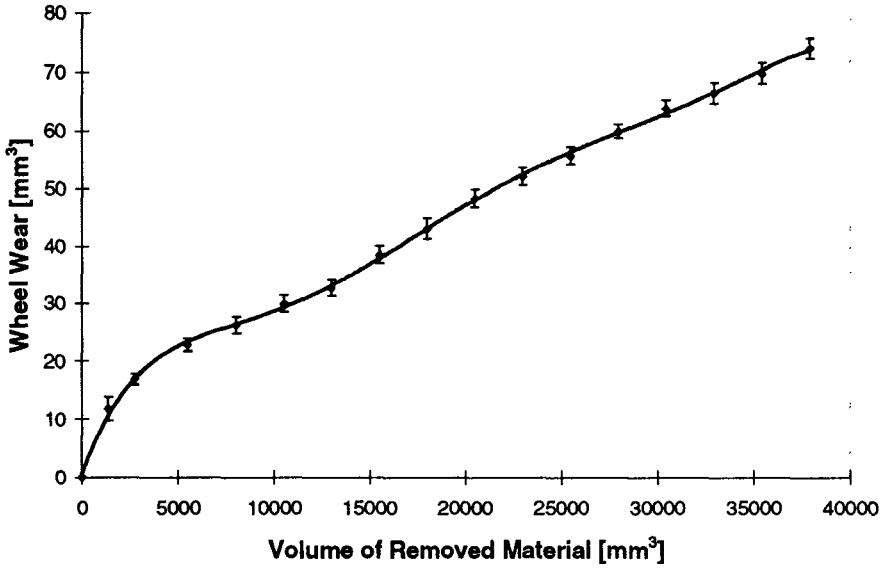

Figure 4.23. Wheel Wear vs. Removed Material for SRBSN -- Large Downfeed

Figure 4.24 is a plot of the G-ratio vs. the volume of removed SRBSN material. The lower G-ratio for this experiment than for that of the previous experiment suggests that increased downfeed reduces the efficiency of the grinding process. The reduced efficiency can be attributed to the softness of the grinding wheel resulting from the increased downfeed and decreased diameter of the grinding wheel (through wear of the wheel) to cause grain fragmentation or bond fracture and the higher wheel-wear rate [Kalpakjian 1991]. A study on the mechanisms of ceramic grinding [Kitajima 1992] showed a similar decrease in the G-ratio for increasing material-removal rates.

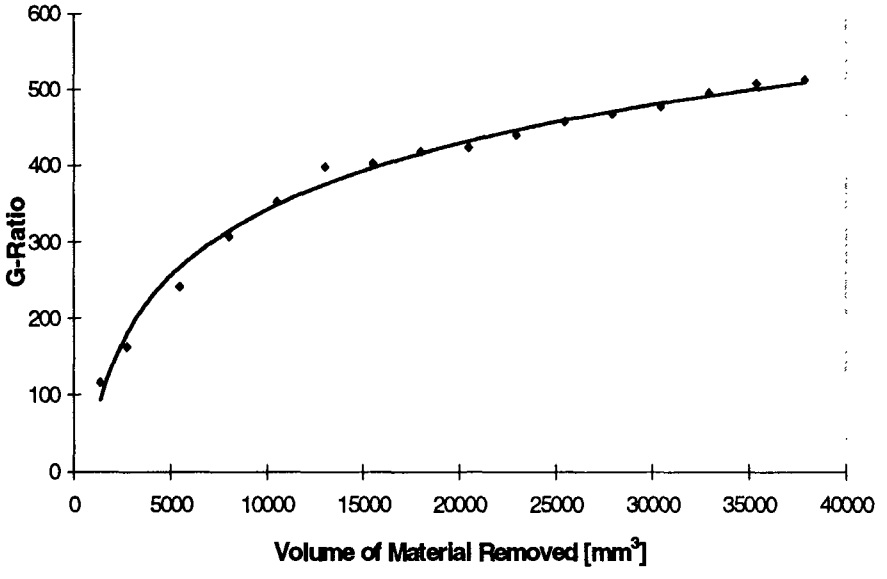

Figure 4.24. G-Ratio for SRBSN -- Large Downfeed

Figure 4.25 is a plot of surface roughness vs. volume of removed SRBSN material. Surface roughness does not change significantly throughout the experiment; values of the surface roughness Ra range from 0.45 to 0.55. The increase in downfeed also has little effect on surface roughness.

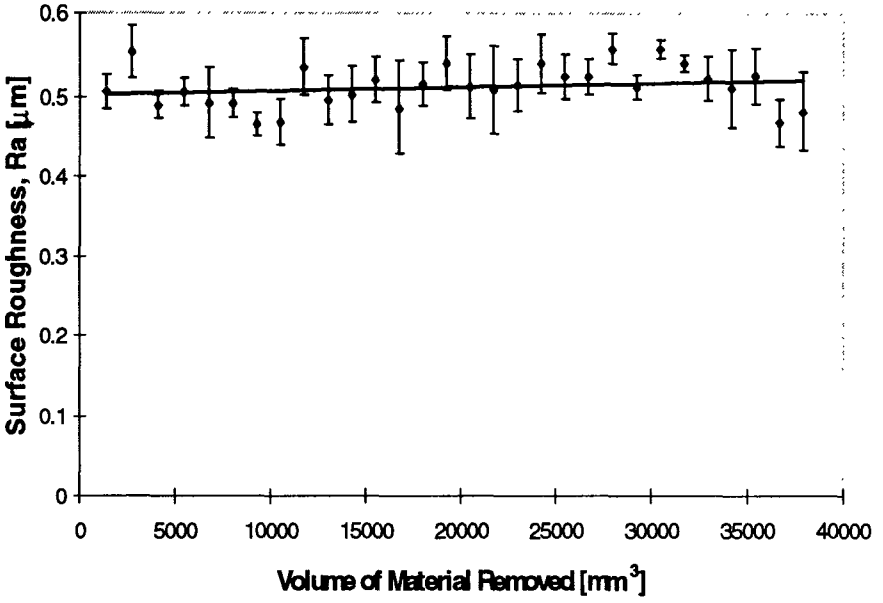

Figure 4.25. Surface Roughness for SRBSN -- Large Downfeed

4.5. Discussion of Results

Figure 4.26 shows that the increase in normal grinding forces as a result of wheel wear is much greater than that of tangential grinding forces. This was also demonstrated by [Spur 1985] when grinding RBSN. The increase in grinding forces may result from failure to dress the grinding wheel after commencing the grinding experiments. The dressing process is necessary to ensure that the tips of diamonds always protrude from the bonding material as the wheel wears. Tsutsumi showed an increase in grinding forces with increasing volume removed in the absence of a dressing process [Tsutsumi 1993]. In-process dressing of the grinding wheel could help to reduce any increase in the grinding forces as the wheel wears.

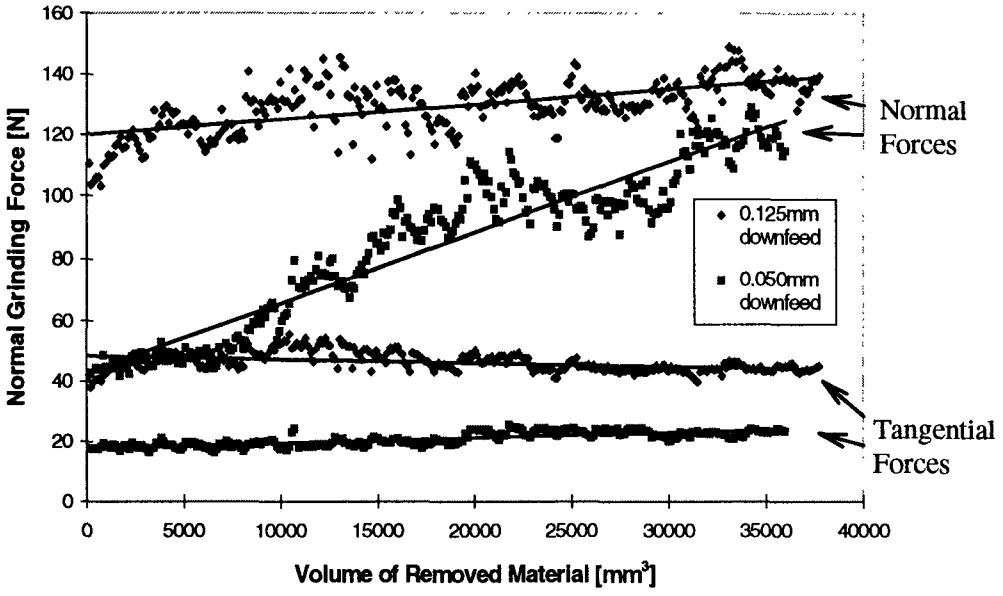

Figure 4.26. Comparison of Grinding Forces for the Experiments at Two Different Downfeeds

The threefold relative increase in normal and tangential grinding force that results from the greater downfeeds corresponds to the nearly threefold increase in material-removal rate from $Q'_w = 6.25$ mm^3/mm•s to $Q'_w = 15.625$ mm^3/mm•s for the 50- and 125-μm downfeeds, respectively. The equation for relative grain force [Kalpakjian 1991]

$$\text{relative grain force} \propto \frac{v}{\mathrm{V\,C}}\sqrt{\frac{d}{D}}$$

where v is workpiece speed, d is downfeed, V is wheel speed, C is number of cutting points, and D is wheel diameter, implies that an increase in downfeed will cause a corresponding increase in force to support these results.

A study by [Subramanian 1985] showed a less significant relative decrease in normal and tangential grinding forces from the low to the high material-removal rates when grinding RBSN. Lower grinding forces would be preferred, as higher forces could produce subsurface damage and, thus, reduce the strength of the part.

Tool-wear curves for single-point cutting tools are readily available. F. W. Taylor showed the relationship between tool life and machining conditions. The parameter of cutting speed for single-point tools has the greatest effect on tool life. Taylor demonstrated the three stages of tool wear -- initial, progressive, and catastrophic. Figure 4.27 shows the tool-wear curve and the three stages of tool wear. Plots of radial wheel wear vs. grinding time during surface grinding have been produced for grinding steels [Verkerk 1974]; however, the Taylor tool-wear curve has not previously been demonstrated for diamond wheels when grinding ceramics.

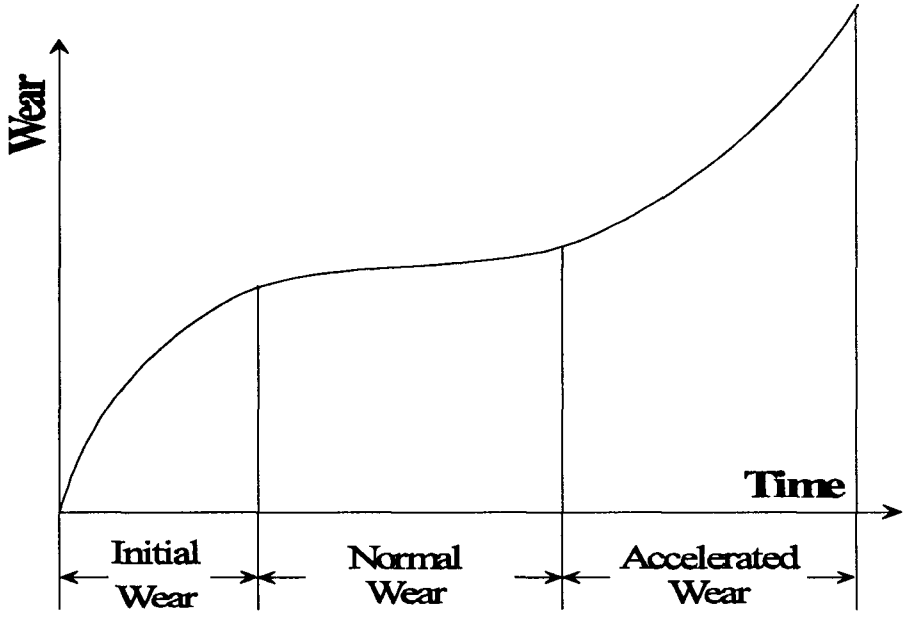

Figure 4.27. Tool-Wear Curve and Three Wear Stages

The most important issue in this research was how to analyze the wheel-wear data. An initial decision was made to plot wheel wear versus the volume of removed material (i.e., silicon nitride) as grinding time was not directly measured during the wear experiments. Figure 4.28 is a plot of wheel wear vs. volume of removed material. Although presentation of the wheel-wear data does not conform to traditional Taylor tool-wear plots, and thus does not exhibit the three wear stages, these plots do show that wheel wear under varying machining conditions is dependent on the volume of material removed.

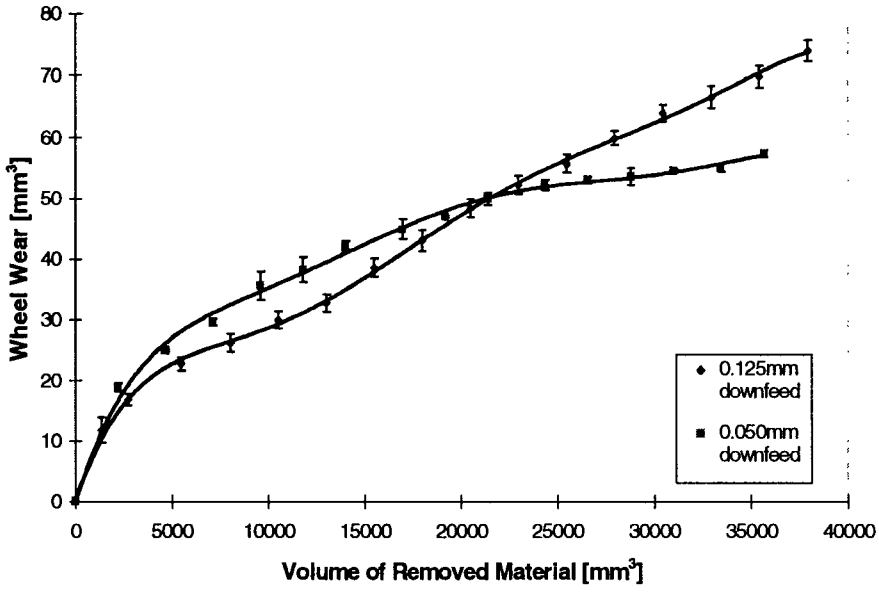

Figure 4.28. Comparison of Wheel-Wear Curves for the Experiments at Two Different Downfeeds vs. Removed Material

Figure 4.29 is a plot of wheel wear vs. grinding time for the small- and large-downfeed experiments. To make this wear plot, a conversion between the grinding time

and the volume of removed material was made based on the machining parameters used. The three wear stages associated with single-point cutting are not present in these plots. The absence of the distinct wear stages suggests that the wear process of the diamond particles differs from the wear of single-point cutting tools. The difference between single-point tools and grinding wheels is that, through the grinding process, the diamond particles become dull, may fracture or become dislodged from the wheel, and may expose new diamond particles. This wear process differs from that of single-point cutting tools where heat build-up associated with large flank wear leads to catastrophic failure of the tool.

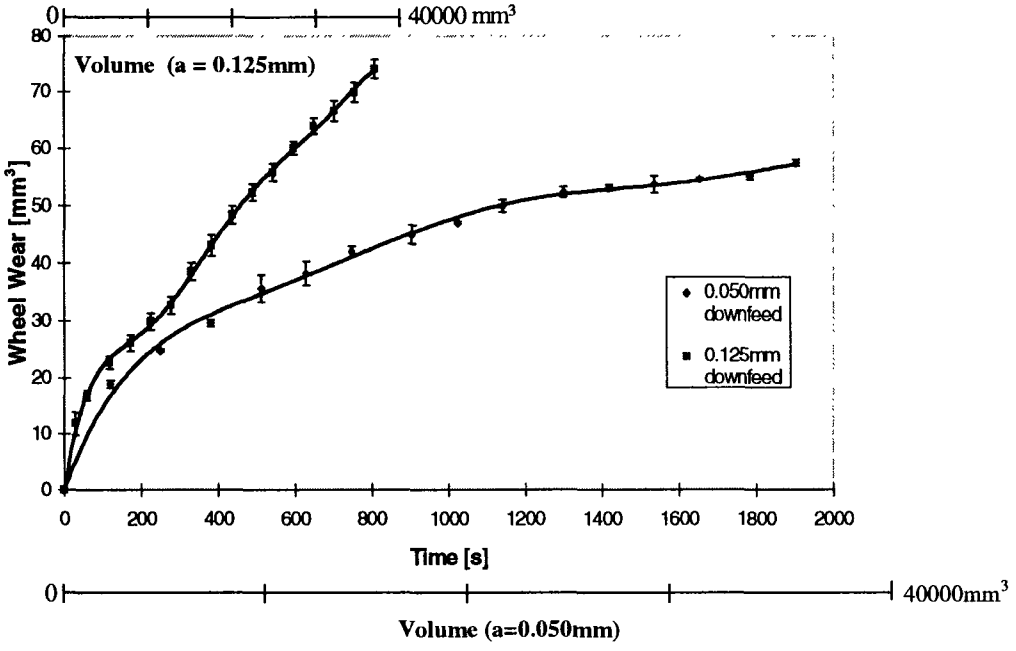

Figure 4.29. Comparison of Wheel Wear Curves for the Experiments at Two Different Downfeeds vs. Grinding Time

The surface roughness of the ceramic materials did not change significantly during the wear experiments. Brinksmeier showed that workpiece-surface roughness during grinding is a function of material-removal rate Q'_w [Brinksmeier 1992]. He showed that the change in workpiece roughness can be insignificant for a twofold increase in Q'w, whereas a fourfold increase in Q'_w can significantly increase the surface roughness. The dependency of surface roughness upon Q'_w may explain the insignificant change in surface roughness than occurs during this experiment where the total material removed during the experiment was very limited.

Chapter 5

Conclusions and Recommendations

5.1. Conclusions

The objective of this thesis research is to investigate wheel wear during grinding of ceramic materials, a subject which has not been explored thoroughly. Recognizing the importance of defining the cost of the grinding process, which is dominated by the cost of the grinding wheel, this research has aimed at developing a methodology to identify the factors contributing to wheel wear as well as the effect of wheel wear on the grinding performance, which in turn determines the productivity of the grinding process and the quality of its result. Significant contributions of this thesis research are:

1. Development of a method to quantitatively measure grinding-wheel wear, using a duplication pattern of the grinding wheel to measure volumetric wheel wear. Experimental results demonstrate that the rate of wheel wear is highest within the first 2000 mm^3 of removed material. Results from this thesis research constitute a unique opportunity for industry to evaluate grinding cost by minimizing the cost of diamond grinding wheels and the cost associated with the truing and dressing processes.

2. The rate of wheel wear is controlled by the machining parameters set for the grinding process. A machining parameter that significantly affects wheel-wear

rate is the downfeed; the experiments have shown that an increase in downfeed causes greater wear of the grinding wheel. A second machining parameter important to wheel-wear rate is the grinding-wheel speed. The tool-life relationship together with the wheel-wear curves will permit selection of optimum machining parameters for a particular grinding process.

3. An important finding of this research under identical grinding conditions:

   (1) Same material: sintered reaction-bonded silicon nitride (SRBSN)

   (2) Downfeed: 50 μm

   (3) Wheel type: 100 concentration wheel, GE RVG-880 diamond

   (4) Spindle speed: ≈3600 RPM

   is that increasing the grinding wheel speed by increasing the diameter of the grinding wheel results in a lower wear rate. This observation is very important for the manufacturing industry. Under precision grinding operations, an alternative way to control the wear rate of the grinding wheel is to increase the diameter of the grinding wheel when there is no other alternative to reduce the grinding wheel wear rate. The lower wear rate is due to the increase in the number of available diamond particles about the circumference of the larger diameter wheel to distribute the wear on the grinding wheel. The disadvantage is the significant increase in the manufacturing cost of the diamond wheel and the cost of trueing and dressing the larger grinding wheel.

4. Material properties are critical in determining the rate of grinding-wheel wear. Results from the initial investigation of grinding sintered reaction-bonded silicon nitride and sintered silicon nitride indicate that the wheel-wear rate for the former is significantly lower than that for the latter. The most important effect of the properties of the material chosen is their relation to the wear rate of the initial wear stage. Observations gained from this investigation indicate that a higher wear rate is associated with materials with a higher wear resistance, such as sintered silicon nitride. The wear resistance can be related to the product of the hardness and toughness of the ceramic workpiece: K_c x H, where K_c is the toughness and H is the hardness [Xu 1996]. The product of K_c x H for SSN is a factor of 2 greater than that of SRBSN if we assign a hardness value of 16 GPa for SRBSN. A material of greater wear resistance would be expected to have a higher wheel-wear rate as the results indicate. Results obtained from this thesis research are the first of their kind having to do with the machining of silicon nitride ceramics.

5.2. Recommendations for Future Studies

To further define the effect of wheel wear on grinding forces and surface roughness, additional experiments could be performed by varying the machining conditions and material selection (e.g., wheel speed, wheel type, table speed, and ceramic material). Use of the design-of-experiments (DOE) technique would produce results

permitting choice of the best combination of conditions to provide the lowest grinding forces and minimized wheel wear.

A Taylor tool-life relationship between wheel speed and wheel wear could be constructed by conducting more wheel-wear experiments at various wheel speeds. A tool-life equation could then be determined for this diamond grinding wheel and silicon nitride ceramic. Inclusion of this information in machining data handbooks would prove invaluable to machine shops in the grinding of silicon nitrides.

The present wheel-wear measurement method is limited in its assumption of a fairly uniform groove profile about the wheel and its use of the circumference of the wheel to calculate wheel wear. A video-imaging technique able to record greater detail in the geometry of the wear groove at fixed intervals about the circumference of the wheel could more precisely calculate the volume of grinding-wheel wear, by integrating the wear-groove volume for the complete revolution (circumference) of the grinding wheel.

Scanning-electron and optical microscopy could be used to study the mechanism of grit and bond wear of the grinding wheel at various stages of wear. A lead-tape impression of the grinding wheel could serve to identify the wear of the diamond grit (fracture or dulling). Use of optical microscopy to study the diamond wheel, however, would lead to difficulty in proper remounting of the wheel and continuation of the experiment.

Appendix A. Software Data-Acquisition Code

The following is the Viewdac digital-acquisition code used to collect and record grinding-force data. The "Settings" subroutine sets the data-collection scan rate. The "Conversion" subroutine initializes the data file. The "Go" subroutine initiates and terminates the data-acquisition program. The "Loop 1" subroutine acquires and plots the 3 channels of grinding-force data. The "Save" subroutine prompts the user to specify the filename and file location to save the data. The "Write" subroutine records the 3 channels of grinding-force data.

```
setup2.seq      Sequence Name

Settings        Block Task
        Settings Begin Begin Task
                scan_rate_input_hz    Numeric Input Task
                        Data: scan_rate hz.2.1.1.1.2.3
                        Panel:  A/D Signal
        Settings End            End Task

Conversion      Block Task
        Conversion Begin        Begin Task
                find dt Numeric Operation Task
                        Operation: X/Y
                        X: 1
                        Y: scanrate_hz.2.1.1.1.2.3
                        Result: dt.2.1.1.1.2.3
                Convert dt to string    String Operation Task
                        R$=Number>String (n, X$)
                        (R$ is the string representation of the number n using X$ as a
                        format string)
                        X$: "11{1000}&0,#### ms/pt"
                        n: dt.2.1.1.1.2.3
                        R$: $dt.2.1.1.1.2.3
                Concatenate $dt         String Operation Task
                        R$=Cat(X$,Y$)
                        (R$ is Y$ catenated (added) to the end of X$)
```

X$: "Time Base"
Y$: $dt.2.1.1.1.2.3
R$: $dtt.2.1.1.1.2.3
Conversion End End Task

Go Toggle Button Task
Data: 0
Panel: A/D Signal
Loop 1 Loop Task
Settings
Start: 0 Stop: 2047 Incr: 1 Current: 1
Infinite (loops continuously until stopped by another task)
Loop 1 Begin Begin Task
A to D1 A/D Task
DAS Device: Das 1600 Board 1
Start Channel: 0 # of Scans: 2048
# of Channels: 3 Scan Rate: scanrate_hz.2.1.1.1.2.3

Ch#	Data Name	Input Range (V)	Slope	Offset
0	A_to_D_1.0.1.2	-10.000 to 9.995	1	0
1	A_to_D_1.1.1	-10.000 to 9.995	1	0
2	A_to_D_1.1.2	-10.000 to 9.995	1	0

Transfer Mode: DMA
Plot_1 Line Graph Task
Y Data Sets X Data Sets
A_to_D_1.0.1.2 vs. index of y

Panel: A/D Signal
Plot_2 Line Graph Task
Y Data Sets X Data Sets
A_to_D_1.1.1 vs. index of y

Panel: A/D Signal

Plot_3 Line Graph Task
Y Data Sets X Data Sets
A_to_D_1.1.2 vs. index of y

Panel: A/D Signal

Loop 1 End End Task
Data File Button Push Button Task
Panel: A/D Signal

Save Button Push Button Task
Panel: Data File Panel

Delete Button Push Button Task
Panel: Data File Panel
CANCEL Button Push Button Task
Panel: Data File Panel
File Name Input String Input Task
Data: $filename.2.1.1.1.2
Panel: Data File Panel
Show Data File Panel Hide/Show Task
Panel: Data File Panel
Hide Data File Panel Hide/Show Task
Panel: Data File Panel
Hide Read_In Plot Panel Hide/Show Task
Panel: Read_In Plots
Show Delete Confirm Hide/Show Task
Panel: Delete Confirm
Hide Delete Confirm Hide/Show Task
Panel: Delete Confirm
Delete YES Button Push Button Task
Panel: Delete Confirm
Delete NO Button Push Button Task
Panel: Delete Confirm

Write Data File ASCII File Write Task

Data List	Type:	Size:
A_to_D_1.0.1.2	Real	2048
A_to_D_1.1.1	Real	2048
A_to_D_1.1.2	Real	2048

File: $filename:2.1.1.1.2
Comment: $dtt.2.1.1.1.2
Column Headings
Line Delimiter: \n CrLf
Column Delimiter: \32
Overwrite

Read Data Block Block Task
Read Data Block Begin Begin Task

Data List:	Type	Size
read_col_1.2	DP.Real	2048
read_col_2.2	DP.Real	2048
read_col_3.2	DP.Real	2048

File: $filename.2.1.1.1.2
Lines Skipped: 2
Line Delimiter: \n CrLf
Column Delimiter: \32 Multiple
Data Format: Auto
Rewind (Read each file from same start position)

Show Read_in Plot Panel Hide/Show Task

Panel: Read_In Plots

Read_In Plot 1 Line Graph Task

Y Data Sets	X Data Sets
read_col_1.2	vs. index of y

Panel: Read_In Plots

Read_In Plot 2 Line Graph Task

Y Data Sets	X Data Sets
read_col_2.2	vs. index of y

Panel: Read_In Plots

Read_In Plot 3 Line Graph Task

Y Data Sets	X Data Sets
read_col_3.2	vs. index of y

Panel: Read_In Plots

Read Data Block End End Task

Hide Read_In Plot Panel Button Push Button Task

Delete Data File DOS Task

File1: $filename.2.1.1.1.2

Operation: Delete

Appendix B. Force-Measurement System Instructions

The following steps are necessary to use the Viewdac data-acquisition program to collect and record grinding-force data.

1. At the DOS prompt C:, type "vd" to launch the VIEWDAC data acquisition application.
2. Under the File menu, select Open\Sequence.
3. Open the setup3.seq file located in the vdv_data directory on drive d.
4. Turn on the KISTLER charge amplifiers; toggle the control switches from reset to operate mode.
5. Click Start push button in the setup3.seq window.
6. Click Scan Rate (Hz) button in A/D Signal window to change sampling rate according to user need.
7. Click On/Off toggle button in A/D Signal window to start acquiring data.
8. Begin grinding tests.
9. Click On/Off toggle button in A/D Signal window to stop acquiring data.
10. Click Data File button in A/D Signal window to display save panel.
11. Save data at the prompt with the following format d:*filename*.prn.
12. Click the Save button in the panel.
13. At the conclusion of the experiments, select the Bye command, under the System menu, to exit the program.
14. Toggle the control switches on the charge amplifiers to the reset position.
15. Turn off the charge amplifiers, oscilloscope, and computer.

Appendix C. Downgrinding Force Data for SRBSN (50 μm Downfeed)

	a = 0.05 mm					Fx = 14.464(Vx)-1.2854								
	v = 0.125 m/s					Fy = 13.717(Vy)+1.4915								
	150 grit					Fz = 32.198(Vz)-0.0332								
	Down Grinding													
[mm^3]	a [mm]	Vx [V]	Vx std	Fx [N]	Fx Std	Vy [V]	Vy std	Fy [N]	Fy std	Vz [V]	Vz std	Fz [N]	Fz std	μ [Fy/Fz]
				Transverse				Tangential				Normal		
249	1000	0	0.223	1.28	1.934	1.168	0.46	17.5	7.805	1.32	0.411	42.6	13.2	0.4109
498	2000	0.01	0.805	1.11	10.36	1.175	0.71	17.6	11.29	1.38	0.902	44.4	29	0.3962
622.5	2500	0.01	0.798	1.15	10.26	1.156	0.74	17.4	11.69	1.36	0.988	43.8	31.8	0.3962
747	3000	0.01	0.767	1.19	9.802	1.21	0.74	18.1	11.67	1.38	0.912	44.4	29.3	0.4079
871.5	3500	0.02	0.787	1	10.1	1.293	0.76	19.2	11.86	1.5	0.885	48.4	28.5	0.3972
996	4000	0.02	0.709	0.93	8.963	1.229	0.73	18.3	11.53	1.39	0.966	44.8	31.1	0.4091
1121	4500	0.02	0.767	0.93	9.814	1.237	0.7	18.5	11.13	1.36	0.831	43.7	26.7	0.4221
1245	5000	0.01	0.759	1.18	9.695	1.208	0.76	18.1	11.91	1.37	0.73	44.1	23.5	0.4093
1370	5500	0.02	0.778	0.97	9.971	1.265	0.6	18.8	9.719	1.47	0.816	47.4	26.3	0.3974
1494	6000	0.03	0.015	0.89	1.063	1.251	0.18	18.7	3.93	1.46	0.008	46.9	0.23	0.3973
1619	6500	0.01	0.575	1.2	7.026	1.188	0.51	17.8	8.478	1.4	0.724	44.9	23.3	0.396
1743	7000	0.02	0.097	1.04	0.12	1.11	0.47	16.7	7.951	1.3	0.308	41.8	9.9	0.4002
1868	7500	0	0.024	1.29	0.932	1.2	0.57	18	9.373	1.38	0.893	44.3	28.7	0.4052
1992	8000	0	0.023	1.24	0.95	1.248	0.58	18.6	9.503	1.44	0.807	46.4	26	0.401
2117	8500	0	0.023	1.28	0.952	1.194	0.57	17.9	9.28	1.37	0.76	44.2	24.4	0.404
2241	9000	0	0.023	1.25	0.954	1.157	0.52	17.4	8.558	1.32	0.651	42.3	20.9	0.4099
2366	9500	0.02	0.447	1.01	5.177	1.3	0.51	19.3	8.427	1.5	0.711	48.2	22.9	0.4011
2490	10000	0.03	0.435	0.91	5.003	1.212	0.5	18.1	8.401	1.44	0.653	46.3	21	0.3917
2615	10500	0.03	0.489	0.87	5.783	1.248	0.48	18.6	8.046	1.53	0.744	49.1	23.9	0.3789
2739	11000	0.04	0.458	0.74	5.345	1.178	0.51	17.7	8.42	1.46	0.744	47.1	23.9	0.3751
2864	11500	0	0.424	1.25	4.854	1.241	0.55	18.5	9.003	1.53	0.755	49.4	24.3	0.375
2988	12000	0.03	0.416	0.87	4.736	1.177	0.57	17.6	9.287	1.49	0.689	47.9	22.1	0.3683
3113	12500	0.02	0.422	1.04	4.812	1.176	0.56	17.6	9.182	1.49	0.693	48.1	22.3	0.3667
3237	13000	0.01	0.417	1.08	4.75	1.073	0.58	16.2	9.439	1.41	0.673	45.4	21.6	0.3574
3362	13500	0.01	0.301	1.09	3.062	1.186	0.63	17.8	10.18	1.4	0.723	45	23.2	0.3948
3486	14000	0	0.322	1.21	3.375	1.178	0.59	17.7	9.569	1.4	0.602	45	19.3	0.3925
3611	14500	0	0.333	1.22	3.536	1.299	0.68	19.3	10.77	1.53	0.674	49.1	21.7	0.3931
3860	15500	0	0.284	1.25	2.816	1.424	0.57	21	9.296	1.64	0.752	52.8	24.2	0.3984
3984	16000	0.02	0.251	1.02	2.34	1.332	0.56	19.8	9.231	1.55	0.65	49.8	20.9	0.3968
4109	16500	0	0.261	1.23	2.496	1.256	0.53	18.7	8.82	1.45	0.653	46.7	21	0.4011
4233	17000	0.01	0.268	1.14	2.591	1.238	0.55	18.5	9.1	1.45	0.682	46.5	21.9	0.3974
4358	17500	0	0.292	1.28	2.937	1.265	0.5	18.8	8.376	1.48	0.626	47.6	20.1	0.3957
4482	18000	0.01	0.314	1.2	3.258	1.242	0.53	18.5	8.764	1.5	0.554	48.3	17.8	0.3837
4607	18500	0.02	0.249	1	2.32	1.189	0.55	17.8	9.018	1.46	0.423	47	13.6	0.3785
4731	19000	0.01	0.281	1.13	2.784	1.173	0.57	17.6	9.299	1.42	0.465	45.8	14.9	0.3836
4856	19500	0	0.293	1.26	2.956	1.136	0.48	17.1	8.082	1.5	0.415	48.3	13.3	0.3532
4980	20000	0.01	0.305	1.15	3.12	1.197	0.54	17.9	8.919	1.42	0.648	45.7	20.8	0.3919
5105	20500	0.02	0.271	1.03	2.633	1.316	0.58	19.5	9.501	1.58	0.668	50.9	21.5	0.3838
5229	21000	0	0.224	1.25	1.955	1.279	0.51	19	8.467	1.49	0.765	47.9	24.6	0.397
5354	21500	0.01	0.224	1.09	1.953	1.319	0.52	19.6	8.69	1.54	0.689	49.6	22.1	0.3952
5478	22000	0	0.232	1.24	2.066	1.321	0.47	19.6	7.99	1.53	0.665	49.2	21.4	0.3989
5603	22500	0.01	0.227	1.19	1.994	1.287	0.45	19.1	7.689	1.53	0.734	49.1	23.6	0.3897
5727	23000	0.01	0.236	1.17	2.126	1.214	0.46	18.1	7.765	1.47	0.568	47.3	18.3	0.3833
5852	23500	0.04	0.273	0.67	2.659	1.279	0.49	19	8.235	1.55	0.683	50	22	0.3807
5976	24000	0	0.345	1.26	3.707	1.224	0.4	18.3	6.934	1.55	0.754	50	24.3	0.3659
6101	24500	0.02	0.361	0.96	3.931	1.177	0.39	17.6	6.842	1.52	0.6	48.8	19.3	0.3615
6225	25000	0	0.35	1.23	3.783	1.217	0.39	18.2	6.85	1.57	0.767	50.5	24.7	0.36
6350	25500	0	0.346	1.21	3.714	1.152	0.35	17.3	6.235	1.46	0.698	47.1	22.4	0.367
6474	26000	0.01	0.31	1.17	3.193	1.117	0.37	16.8	6.542	1.53	0.664	49.3	21.3	0.3413
6599	26500	0.01	0.384	1.21	4.266	1.066	0.4	16.1	6.997	1.37	0.65	43.9	20.9	0.3667
6723	27000	0.02	0.443	0.99	5.129	1.159	0.5	17.4	8.341	1.4	0.666	45.1	21.4	0.3855
6848	27500	0.02	0.494	0.95	5.853	1.285	0.46	19.1	7.869	1.59	0.738	51.1	23.7	0.3745
6972	28000	0.02	0.536	0.98	6.47	1.247	0.46	18.6	7.798	1.49	0.749	48	24.1	0.3871
7097	28500	0.01	0.436	1.17	5.02	1.212	0.49	18.1	8.241	1.47	0.661	47.3	21.3	0.3828
7221	29000	0.01	0.358	1.18	3.889	1.348	0.58	20	9.417	1.63	0.853	52.5	27.4	0.3803
7346	29500	0.01	0.328	1.14	3.458	1.3	0.48	19.3	8.066	1.58	0.775	51	24.9	0.3792
7470	30000	0.03	0.308	0.91	3.168	1.209	0.56	18.1	9.107	1.56	0.721	50.2	23.2	0.3603
7595	30500	0.02	0.318	0.96	3.317	1.231	0.51	18.4	8.456	1.58	0.859	50.7	27.6	0.3625
7719	31000	0	0.326	1.25	3.433	1.278	0.46	19	7.812	1.68	0.762	54	24.5	0.3524
7844	31500	0.02	0.338	1.04	3.601	1.257	0.52	18.7	8.571	1.7	0.78	54.9	25.1	0.3417
7968	32000	0	0.387	1.27	4.312	1.191	0.45	17.8	7.691	1.66	0.756	53.4	24.3	0.3337
8093	32500	0.01	0.411	1.18	4.656	1.117	0.43	16.8	7.356	1.57	0.827	50.5	26.6	0.3327
8217	33000	0.03	0.491	0.87	5.82	1.201	0.41	18	7.177	1.65	0.778	53.2	25	0.3374

8217	33000	0.03	0.491	0.87	5.82	1.201	0.41	18	7.177	1.65	0.778	53.2	25	0.3374
8342	33500	0.02	0.461	0.94	5.378	1.262	0.43	18.8	7.323	1.78	0.741	57.2	23.8	0.3288
8466	34000	0	0.436	1.26	5.028	1.257	0.46	18.7	7.736	1.76	0.812	56.7	26.1	0.3302
8591	34500	0.01	0.445	1.11	5.152	1.3	0.46	19.3	7.761	1.85	0.846	59.4	27.2	0.3253
8715	35000	0.01	0.46	1.13	5.365	1.275	0.42	19	7.218	1.83	0.755	58.9	24.3	0.322
8840	35500	0.02	0.449	0.97	5.211	1.312	0.46	19.5	7.849	1.9	0.747	61.2	24	0.3182
8964	36000	0.01	0.47	1.08	5.508	1.281	0.45	19.1	7.606	1.84	0.718	59.2	23.1	0.322
9089	36500	0.02	0.489	0.93	5.781	1.343	0.44	19.9	7.487	1.98	0.702	63.6	22.6	0.3131
9213	37000	0.02	0.496	1	5.883	1.335	0.41	19.8	7.162	1.9	0.718	61.2	23.1	0.3235
9338	37500	0.01	0.556	1.08	6.763	1.353	0.44	20	7.533	1.99	0.712	64.1	22.9	0.3127
9462	38000	0.01	0.553	1.14	6.715	1.355	0.42	20.1	7.273	2.02	0.837	65	26.9	0.3088
9587	38500	0.02	0.552	1.07	6.694	1.385	0.44	20.5	7.519	2.05	0.699	65.8	22.5	0.3113
9711	39000	0.01	0.566	1.1	6.908	1.328	0.4	19.7	7.007	1.99	0.968	64.1	31.1	0.3075
9836	39500	0.02	0.728	0.99	9.242	1.213	0.42	18.1	7.186	1.66	0.693	53.5	22.3	0.3389
9960	40000	0.08	0.725	0.13	9.199	1.156	0.44	17.4	7.463	1.75	0.682	56.3	21.9	0.3084
10085	40500	0.07	0.723	0.34	9.174	1.18	0.49	17.7	8.215	1.86	0.612	60	19.7	0.2946
10209	41000	0.04	0.669	0.66	8.391	1.207	0.51	18.1	8.531	1.92	0.63	61.7	20.3	0.2926
10334	41500	0.09	0.771	0.07	9.866	1.142	0.38	17.2	6.73	1.94	0.823	62.4	26.5	0.2747
10458	42000	0.09	0.772	0.03	9.884	1.217	0.41	18.2	7.152	2.04	0.826	65.6	26.5	0.2774
10583	42500	0.08	0.811	0.17	10.45	1.56	0.48	22.9	8.093	2.27	0.897	73.2	28.9	0.3128
10707	43000	0.07	0.664	0.27	8.314	1.658	0.56	24.2	9.139	2.47	0.784	79.4	25.2	0.3052
10956	44000	0.07	0.771	0.35	9.869	1.203	0.41	18	7.084	2.2	0.765	70.9	24.6	0.2536
11081	44500	0.03	0.789	0.78	10.12	1.222	0.42	18.3	7.321	2.19	0.84	70.5	27	0.2588
11205	45000	0.05	0.829	0.61	10.7	1.215	0.39	18.2	6.806	2.26	0.773	72.8	24.9	0.2492
11330	45500	0.05	0.755	0.52	9.642	1.226	0.37	18.3	6.58	2.21	0.726	71.1	23.3	0.2576
11454	46000	0.06	0.808	0.46	10.4	1.212	0.49	18.1	8.22	2.28	0.918	73.3	29.5	0.2471
11579	46500	0.06	0.724	0.38	9.189	1.249	0.52	18.6	8.566	2.31	0.771	74.5	24.8	0.25
11703	47000	0.04	0.643	0.74	8.011	1.212	0.49	18.1	8.28	2.26	0.861	72.9	27.7	0.2485
11828	47500	0.08	0.734	0.16	9.332	1.247	0.48	18.6	8.077	2.37	0.876	76.4	28.2	0.2435
11952	48000	0.04	0.719	0.72	9.117	1.28	0.49	19.1	8.178	2.51	0.803	80.8	25.8	0.2357
12077	48500	0.04	0.734	0.71	9.329	1.243	0.49	18.5	8.171	2.32	0.807	74.7	26	0.2481
12201	49000	0.1	0.633	0.14	7.878	1.28	0.43	19.1	7.404	2.34	0.746	75.4	24	0.2529
12326	49500	0.1	0.642	0.15	7.997	1.228	0.41	18.3	7.122	2.33	0.797	75	25.6	0.2445
12450	50000	0.01	0.726	1.1	9.212	1.227	0.4	18.3	7.027	2.31	0.899	74.3	28.9	0.2466
12575	50500	0.07	0.719	0.3	9.118	1.282	0.39	19.1	6.901	2.45	0.859	79	27.6	0.2416
12699	51000	0.06	0.742	0.41	9.449	1.297	0.39	19.3	6.886	2.48	0.98	80	31.5	0.2411
12824	51500	0	0.698	1.24	8.813	1.45	0.41	21.4	7.118	2.31	0.879	74.3	28.3	0.2877
12948	52000	0.01	0.689	1.08	8.682	1.374	0.39	20.3	6.845	2.21	0.814	71.2	26.2	0.2857
13073	52500	0.03	0.536	0.89	6.465	1.379	0.44	20.4	7.531	2.22	0.66	71.3	21.2	0.286
13197	53000	0.01	0.562	1.2	6.846	1.412	0.37	20.9	6.596	2.26	0.69	72.7	22.2	0.287
13322	53500	0.01	0.542	1.17	6.559	1.301	0.42	19.3	7.198	2.19	0.539	70.4	17.3	0.2748
13446	54000	0.02	0.538	0.98	6.503	1.305	0.42	19.4	7.304	2.2	0.725	70.8	23.3	0.274
13571	54500	0.05	0.535	0.58	6.451	1.258	0.37	18.7	6.619	2.09	0.799	67.4	25.7	0.2782
13695	55000	0	0.503	1.25	5.997	1.28	0.36	19	6.396	2.21	0.627	71.2	20.1	0.2674
13820	55500	0.03	0.507	0.9	6.053	1.222	0.39	18.3	6.807	2.18	0.623	70.2	20	0.2599
13944	56000	0.01	0.519	1.09	6.222	1.266	0.36	18.9	6.472	2.33	0.766	74.9	24.6	0.2518
14069	56500	0.01	0.525	1.07	6.314	1.312	0.43	19.5	7.39	2.36	0.664	76.1	21.3	0.2562
14193	57000	0.03	0.586	0.78	7.187	1.287	0.46	19.1	7.859	2.42	0.828	78	26.6	0.2455
14318	57500	0.01	0.559	1.15	6.799	1.197	0.4	17.9	6.971	2.33	0.581	75.1	18.7	0.2385
14442	58000	0	0.575	1.25	7.03	1.307	0.51	19.4	8.518	2.46	0.887	79.2	28.5	0.2451
14567	58500	0.01	0.575	1.11	7.025	1.267	0.4	18.9	6.947	2.54	0.676	81.7	21.7	0.231
14691	59000	0.02	0.519	0.96	6.223	1.387	0.46	20.5	7.766	2.69	0.959	86.6	30.8	0.2369
14816	59500	0.01	0.549	1.18	6.661	1.46	0.49	21.5	8.249	2.71	1.015	87.2	32.6	0.2467
14940	60000	0.01	0.529	1.14	6.365	1.418	0.46	20.9	7.844	2.64	0.983	84.9	31.6	0.2466
15065	60500	0.04	0.5	0.68	5.944	1.426	0.52	21.1	8.647	2.64	1.067	85	34.3	0.2477
15189	61000	0.02	0.488	1.05	5.774	1.338	0.5	19.8	8.326	2.57	1.023	82.7	32.9	0.2401
15314	61500	0.02	0.453	0.99	5.273	1.351	0.43	20	7.397	2.74	0.882	88.2	28.4	0.227
15438	62000	0.02	0.452	1.06	5.258	1.303	0.41	19.4	7.18	2.61	0.979	83.8	31.5	0.231
15563	62500	0.04	0.478	0.69	5.633	1.324	0.43	19.7	7.344	2.72	1.093	87.7	35.2	0.2242
15687	63000	0.03	0.437	0.87	5.034	1.304	0.46	19.4	7.783	2.77	1.029	89.2	33.1	0.2171
15812	63500	0.03	0.458	0.86	5.344	1.391	0.48	20.6	8.009	2.94	1.023	94.6	32.9	0.2175
15936	64000	0.04	0.441	0.77	5.099	1.403	0.47	20.7	7.896	2.91	1.026	93.7	33	0.2212
16061	64500	0.05	0.445	0.61	5.152	1.416	0.5	20.9	8.315	3.06	1.02	98.5	32.8	0.2123
16185	65000	0.02	0.505	0.96	6.019	1.356	0.43	20.1	7.344	2.98	1.004	96	32.3	0.2093
16310	65500	0.01	0.676	1.19	8.493	1.308	0.56	19.4	9.153	2.7	1.123	86.8	36.1	0.2239
16434	66000	0.02	0.669	0.98	8.397	1.345	0.55	19.9	8.976	2.85	1.135	91.7	36.5	0.2176
16559	66500	0.01	0.751	1.07	9.574	1.372	0.55	20.3	8.989	2.88	1.14	92.8	36.7	0.2189
16683	67000	0.02	0.801	0.98	10.3	1.292	0.42	19.2	7.282	2.8	1.142	90.1	36.7	0.2134
16808	67500	0.01	0.881	1.2	11.46	1.288	0.5	19.2	8.395	2.79	1.081	89.8	34.8	0.2135
16932	68000	0.04	0.902	0.69	11.76	1.245	0.47	18.6	8.003	2.75	1.097	88.4	35.3	0.2101
17057	68500	0.05	0.961	0.55	12.61	1.25	0.49	18.6	8.18	2.67	1.16	85.9	37.3	0.2169

17306	69500	0.02	1.109	0.98	14.76	1.187	0.51	17.8	8.446	2.66	1.15	85.7	37	0.2074
17430	70000	0.03	1.132	0.91	15.08	1.251	0.61	18.7	9.88	2.76	1.113	88.9	35.8	0.2098
17555	70500	0.03	1.145	0.79	15.27	1.274	0.59	19	9.563	2.88	1.155	92.6	37.2	0.2048
17679	71000	0.07	1.197	0.3	16.03	1.277	0.61	19	9.815	2.92	1.172	94	37.7	0.2022
17804	71500	0.01	1.241	1.11	16.67	1.299	0.58	19.3	9.459	2.85	1.012	91.8	32.5	0.2104
17928	72000	0.02	1.317	1.02	17.76	1.434	0.7	21.2	11.07	2.99	1.089	96.1	35	0.2202
18053	72500	0	1.369	1.26	18.51	1.396	0.75	20.6	11.84	2.97	1.074	95.7	34.6	0.2157
18177	73000	0.05	1.271	0.6	17.1	1.349	0.73	20	11.46	2.97	1.217	95.7	39.1	0.209
18302	73500	0	1.337	1.25	18.06	1.35	0.73	20	11.52	2.87	1.083	92.3	34.8	0.2169
18426	74000	0.01	1.251	1.2	16.81	1.373	0.75	20.3	11.8	2.85	0.994	91.6	32	0.2218
18551	74500	0.03	1.259	0.79	16.92	1.359	0.69	20.1	11.02	2.8	0.895	90.3	28.8	0.2231
18675	75000	0.04	1.269	0.69	17.07	1.266	0.75	18.9	11.73	2.7	0.999	86.8	32.1	0.2173
18800	75500	0.05	1.162	0.59	15.52	1.259	0.72	18.8	11.35	2.71	0.919	87.3	29.6	0.2151
18924	76000	0.05	1.049	0.53	13.89	1.305	0.6	19.4	9.733	2.76	0.67	88.7	21.5	0.2186
19049	76500	0.01	1.156	1.21	15.43	1.273	0.64	18.9	10.31	2.84	0.847	91.3	27.2	0.2075
19173	77000	0.08	1.137	0.16	15.15	1.322	0.65	19.6	10.34	2.91	0.953	93.6	30.6	0.2097
19298	77500	0.02	0.988	0.94	13.01	1.363	0.56	20.2	9.136	2.87	0.7	92.5	22.5	0.2183
19422	78000	0.03	1.083	0.9	14.38	1.358	0.58	20.1	9.408	2.97	0.728	95.5	23.4	0.2106
19547	78500	0.04	0.682	0.68	8.583	1.537	0.94	22.6	14.36	3.26	1.809	105	58.2	0.2149
19671	79000	0.06	0.587	0.36	7.204	1.444	0.85	21.3	13.18	3.08	1.756	99.1	56.5	0.215
19796	79500	0.08	1.085	0.19	14.41	1.634	0.64	23.9	10.31	3.45	1.062	111	34.1	0.2149
19920	80000	0.06	0.864	0.41	11.21	1.634	0.92	23.9	14.13	3.42	1.799	110	57.9	0.2173
20045	80500	0.05	0.985	0.5	12.96	1.641	0.84	24	13.06	3.42	1.671	110	53.8	0.2181
20169	81000	0.05	0.962	0.55	12.62	1.638	0.74	24	11.71	3.36	1.334	108	42.9	0.2213
20294	81500	0.01	0.707	1.07	8.942	1.605	0.93	23.5	14.24	3.32	1.76	107	56.6	0.2198
20418	82000	0.02	0.634	0.95	7.888	1.608	0.93	23.5	14.22	3.26	1.601	105	51.5	0.2244
20543	82500	0.02	0.791	0.95	10.15	1.636	0.94	23.9	14.32	3.33	1.684	107	54.2	0.2234
20667	83000	0.03	0.729	0.8	9.257	1.585	0.92	23.2	14.05	3.13	1.675	101	53.9	0.2305
20792	83500	0.03	0.73	0.9	9.276	1.622	0.96	23.7	14.63	3.25	1.708	105	55	0.2272
20916	84000	0.02	0.033	0.94	0.812	1.535	0.38	22.5	6.668	3.1	0.015	99.7	0.46	0.226
21041	84500	0.03	0.016	0.91	1.049	1.497	0.01	22	1.662	2.97	0.007	95.6	0.19	0.2304
21165	85000	0.01	0.439	1.07	5.07	1.426	0.9	21.1	13.77	2.87	1.634	92.4	52.6	0.2278
21290	85500	0.04	0.015	0.75	1.062	1.381	0.39	20.4	6.901	2.85	0.008	91.7	0.22	0.2228
21414	86000	0.04	0.039	0.72	0.715	1.539	0.39	22.6	6.871	3.2	0.016	103	0.48	0.2194
21539	86500	0.04	0.729	0.76	9.258	1.493	0.78	22	12.24	3.04	1.234	97.7	39.7	0.2248
21663	87000	0.05	0.034	0.61	0.798	1.515	0.39	22.3	6.89	3.14	0.011	101	0.33	0.2203
21788	87500	0.07	0.237	0.33	2.137	1.74	0.69	25.4	10.92	3.55	1.059	114	34.1	0.222
21912	88000	0.04	0.025	0.77	0.924	1.702	0.4	24.8	6.932	3.47	0.013	112	0.38	0.2223
22037	88500	0.02	0.367	0.94	4.017	1.672	0.73	24.4	11.44	3.33	1.419	107	45.6	0.2277
22161	89000	0.04	0.032	0.67	0.826	1.687	0.41	24.6	7.058	3.31	0.014	107	0.42	0.231
22286	89500	0.03	0.235	0.81	2.114	1.641	0.56	24	9.153	3.23	1.003	104	32.3	0.2305
22410	90000	0.03	0.203	0.81	1.646	1.668	0.47	24.4	8	3.25	0.951	105	30.6	0.2331
22535	90500	0.05	0.401	0.52	4.511	1.606	0.73	23.5	11.45	3.09	1.332	99.4	42.8	0.2367
22659	91000	0.03	0.029	0.79	0.866	1.487	0.41	21.9	7.067	2.94	0.013	94.7	0.4	0.2312
22784	91500	0.03	0.016	0.81	1.058	1.504	0.43	22.1	7.388	2.96	0.008	95.4	0.22	0.232
22908	92000	0.05	0.475	0.58	5.585	1.436	0.88	21.2	13.57	2.83	1.589	91.1	51.1	0.2326
23033	92500	0.04	0.389	0.71	4.341	1.579	0.86	23.2	13.28	3.18	1.489	102	47.9	0.226
23157	93000	0.02	0.158	0.99	0.998	1.604	0.33	23.5	5.953	3.17	0.564	102	18.1	0.2301
23282	93500	0.03	0.361	0.85	3.936	1.673	0.82	24.4	12.71	3.25	1.429	105	46	0.2335
23406	94000	0.01	0.03	1.14	0.854	1.631	0.42	23.9	7.198	3.21	0.015	103	0.44	0.2311
23531	94500	0.02	0.016	1	1.06	1.652	0.44	24.2	7.531	3.22	0.009	104	0.27	0.2334
23655	95000	0.01	0.026	1.12	0.902	1.676	0.07	24.5	2.488	3.23	0.013	104	0.4	0.2357
23780	95500	0.02	0.436	1.05	5.018	1.622	0.96	23.7	14.71	3.14	1.587	101	51.1	0.2348
23904	96000	0	0.022	1.28	0.969	1.624	0.37	23.8	6.629	3.09	0.012	99.6	0.34	0.2386
24029	96500	0.01	0.026	1.13	0.911	1.624	0.4	23.8	6.912	3.09	0.012	99.5	0.34	0.2388
24153	97000	0.02	0.032	1.01	0.828	1.624	0.38	23.8	6.679	2.97	0.013	95.6	0.4	0.2486
24278	97500	0	0.025	1.22	0.922	1.467	0.4	21.6	6.985	2.81	0.011	90.3	0.31	0.2394
24402	98000	0.02	0.328	1.07	3.457	1.529	0.64	22.5	10.22	2.92	1.094	94	35.2	0.2392
24527	98500	0.02	0.559	1	6.803	1.609	1.01	23.6	15.41	3.1	1.658	99.8	53.3	0.236
24651	99000	0.03	0.804	0.79	10.34	1.643	0.91	24	13.97	3.12	1.039	100	33.4	0.2393
24776	99500	0.01	0.712	1.15	9.017	1.66	1.01	24.3	15.4	3.13	1.55	101	49.9	0.2408
24900	1E+05	0.02	0.507	0.96	6.047	1.65	0.95	24.1	14.54	3.05	1.541	98.2	49.6	0.2458
25025	1E+05	0.02	0.669	0.99	8.388	1.659	1.03	24.3	15.62	3.13	1.518	101	48.9	0.2409
25149	1E+05	0.02	0.522	0.93	6.269	1.664	0.97	24.3	14.84	3.12	1.646	100	53	0.2421
25274	1E+05	0.02	0.016	1.03	1.056	1.611	0.46	23.6	7.86	2.97	0.008	95.7	0.23	0.2466
25398	1E+05	0.04	0.094	0.71	0.074	1.572	0.39	23.1	6.881	2.99	0.08	96.1	2.55	0.24
25523	1E+05	0.03	0.365	0.86	3.998	1.602	0.81	23.5	12.55	3	1.239	96.6	39.9	0.2428
25647	1E+05	0.01	0.576	1.2	7.04	1.568	0.97	23	14.83	2.97	1.528	95.6	49.2	0.2406
25772	1E+05	0.01	0.428	1.09	4.902	1.512	0.82	22.2	12.75	2.85	1.351	91.9	43.5	0.2419
25896	1E+05	0.01	0.612	1.11	7.567	1.484	0.89	21.8	13.65	2.7	1.467	87	47.2	0.251
26021	1E+05	0.01	0.75	1.09	9.561	1.432	0.86	21.1	13.27	2.73	1.502	87.9	48.3	0.2404

26021	1E+05	0.01	0.75	1.09	9.561	1.432	0.86	21.1	13.27	2.73	1.502	87.9	48.3	0.2404
26145	1E+05	0	0.897	1.25	11.69	1.474	0.88	21.7	13.6	2.79	1.487	89.7	47.9	0.242
26270	1E+05	0.01	0.189	1.1	1.454	1.639	0.49	24	8.28	3.06	0.359	98.6	11.5	0.2433
26394	1E+05	0.01	0.603	1.08	7.43	1.564	0.87	22.9	13.38	3.08	1.443	99.1	46.4	0.2316
26519	1E+05	0.01	0.029	1.12	0.863	1.566	0.41	23	7.179	2.97	0.01	95.4	0.3	0.2407
26643	1E+05	0	0.555	1.23	6.743	1.64	0.81	24	12.59	3.06	1.373	98.4	44.2	0.2437
26768	1E+05	0	0.668	1.27	8.382	1.66	0.89	24.3	13.71	3.04	1.568	97.9	50.5	0.2477
26892	1E+05	0	1.035	1.22	13.68	1.56	0.66	22.9	10.57	2.92	0.924	94	29.7	0.2434
27017	1E+05	0.04	0.017	0.78	1.041	1.621	0.44	23.7	7.55	3.06	0.009	98.5	0.24	0.2409
27141	1E+05	0.01	0.478	1.17	5.629	1.618	0.71	23.7	11.28	3.05	1.244	98	40	0.2417
27266	1E+05	0.02	0.033	0.92	0.814	1.592	0.48	23.3	8.04	2.98	0.011	95.9	0.32	0.2433
27390	1E+05	0.01	0.556	1.15	6.753	1.646	0.75	24.1	11.74	3.03	1.306	97.6	42	0.2465
27515	1E+05	0.02	0.968	0.98	12.71	1.498	0.77	22	12.08	2.73	1.199	87.7	38.6	0.2512
27639	1E+05	0.04	0.979	0.69	12.88	1.562	0.93	22.9	14.26	3.01	1.655	96.9	53.3	0.2366
27764	1E+05	0.02	0.858	1.01	11.13	1.537	0.93	22.6	14.25	3.02	1.687	97.3	54.3	0.232
27888	1E+05	0.02	0.875	1	11.37	1.629	0.97	23.8	14.83	3.13	1.658	101	53.4	0.2365
28013	1E+05	0.02	0.866	1.04	11.23	1.664	0.95	24.3	14.59	3.27	1.722	105	55.4	0.2309
28137	1E+05	0.03	0.552	0.84	6.699	1.655	0.8	24.2	12.46	3.23	1.323	104	42.6	0.233
28262	1E+05	0.03	1.071	0.84	14.21	1.659	0.95	24.3	14.57	3.19	1.586	103	51	0.2361
28386	1E+05	0.02	0.476	1	5.594	1.611	0.75	23.6	11.84	3.08	1.024	99	32.9	0.2382
28511	1E+05	0.01	0.645	1.13	8.049	1.599	0.77	23.4	12.1	3.04	1.384	98	44.5	0.2391
28635	1E+05	0.01	0.889	1.18	11.57	1.675	0.99	24.5	15.08	3.22	1.658	104	53.4	0.236
28760	1E+05	0.01	1.068	1.17	14.16	1.606	0.95	23.5	14.57	3.04	1.496	97.8	48.1	0.2406
28884	1E+05	0.03	0.9	0.86	11.73	1.605	0.99	23.5	15.05	3.26	1.671	105	53.8	0.2242
29009	1E+05	0.02	0.917	1.04	11.97	1.587	0.96	23.3	14.72	2.97	1.589	95.7	51.1	0.243
29133	1E+05	0.02	0.015	0.97	1.068	1.439	0.01	21.2	1.657	2.84	0.006	91.5	0.17	0.2321
29258	1E+05	0.07	0.044	0.26	0.653	1.528	0.39	22.4	6.882	2.94	0.014	94.5	0.43	0.2375
29382	1E+05	0.05	0.039	0.59	0.723	1.485	0.45	21.9	7.641	2.93	0.009	94.4	0.25	0.2316
29507	1E+05	0.06	0.481	0.37	5.669	1.464	0.66	21.6	10.55	2.95	1.265	94.8	40.7	0.2275
29631	1E+05	0.05	0.021	0.52	0.978	1.477	0.43	21.7	7.366	2.98	0.011	96	0.33	0.2265
29756	1E+05	0.07	0.032	0.25	0.823	1.456	0.43	21.5	7.451	3.15	0.01	101	0.28	0.2117
29880	1E+05	0.06	0.017	0.38	1.034	1.441	0.42	21.3	7.246	2.99	0.007	96.3	0.19	0.2207
30005	1E+05	0.1	0.028	0.09	0.885	1.342	0.43	19.9	7.392	2.98	0.011	96	0.33	0.2072
30129	1E+05	0.06	1.126	0.36	15.01	1.348	0.78	20	12.25	3.04	0.956	98	30.8	0.2039
30254	1E+05	0.05	0.423	0.59	4.837	1.412	0.47	20.9	7.998	3.23	1.018	104	32.7	0.2005
30378	1E+05	0.06	0.024	0.35	0.931	1.419	0.42	21	7.317	3.26	0.013	105	0.37	0.1995
30503	1E+05	0.12	0.016	0.45	1.05	1.451	0.43	21.4	7.411	3.33	0.008	107	0.22	0.1999
30627	1E+05	0.04	0.76	0.71	9.709	1.564	1.1	22.9	16.61	3.74	2.033	120	65.4	0.1908
30752	1E+05	0.1	1.227	0.09	16.46	1.52	0.79	22.3	12.33	3.54	1.093	114	35.1	0.196
30876	1E+05	0.04	0.591	0.78	7.268	1.505	0.85	22.1	13.08	3.56	1.701	115	54.7	0.1932
31001	1E+05	0.03	0.328	0.82	3.455	1.548	0.55	22.7	9.041	3.5	1.117	113	35.9	0.2015
31125	1E+05	0.04	0.523	0.75	6.283	1.443	0.83	21.3	12.82	3.37	1.594	109	51.3	0.1959
31250	1E+05	0.02	0.911	1.01	11.89	1.583	0.98	23.2	15	3.76	1.851	121	59.6	0.1918
31374	1E+05	0.05	0.015	0.6	1.062	1.558	0.01	22.9	1.663	3.61	0.007	116	0.19	0.1965
31499	1E+05	0.02	0.132	1.01	0.628	1.59	0.27	23.3	5.242	3.72	0.478	120	15.4	0.1944
31623	1E+05	0.01	0.017	1.12	1.035	1.537	0.01	22.6	1.676	3.61	0.007	116	0.2	0.1941
31748	1E+05	0.04	0.604	0.72	7.444	1.531	0.95	22.5	14.49	3.74	1.93	120	62.1	0.1871
31872	1E+05	0.03	0.317	0.82	3.303	1.542	0.62	22.6	9.965	3.53	1.306	114	42	0.1992
31997	1E+05	0.02	0.29	1.05	2.911	1.563	0.65	22.9	10.47	3.77	1.262	121	40.6	0.1892
32121	1E+05	0.02	1.074	1.03	14.25	1.513	1	22.2	15.19	3.69	1.073	119	34.5	0.1871
32246	1E+05	0.01	0.848	1.17	10.98	1.581	1.12	23.2	16.89	3.9	1.925	125	61.9	0.1848
32370	1E+05	0.04	0.76	0.71	9.709	1.564	1.1	22.9	16.61	3.74	2.033	120	65.4	0.1908
32495	1E+05	0.07	0.036	0.33	0.758	1.57	0.42	23	7.271	3.76	0.012	121	0.35	0.1903
32619	1E+05	0.07	0.651	0.21	8.126	1.519	1.17	22.3	17.51	3.73	1.952	120	62.8	0.1861
32744	1E+05	0.08	0.319	0.15	3.324	1.514	0.61	22.3	9.925	3.61	1.325	116	42.6	0.1913
32868	1E+05	0.07	0.722	0.29	9.161	1.503	1.11	22.1	16.65	3.67	1.783	118	57.4	0.187
32993	1E+05	0.06	0.428	0.35	4.905	1.517	0.85	22.3	13.21	3.63	1.685	117	54.2	0.1909
33117	1E+05	0.03	0.337	0.87	3.585	1.417	0.53	20.9	8.706	3.45	1.035	111	33.3	0.1884
33242	1E+05	0.06	0.574	0.39	7.023	1.422	1.06	21	16.02	3.42	1.902	110	61.2	0.1908
33366	1E+05	0.05	0.304	0.49	3.114	1.401	0.76	20.7	11.96	3.38	1.457	109	46.9	0.1905
33491	1E+05	0.05	0.25	0.57	2.325	1.49	0.62	21.9	10	3.59	1.224	116	39.4	0.1896
33615	1E+05	0.06	0.24	0.46	2.191	1.477	0.53	21.7	8.792	3.62	1.037	116	33.4	0.1867
33740	1E+05	0.06	0.359	0.46	3.913	1.507	0.82	22.2	12.72	3.63	1.645	117	52.9	0.1898
33864	1E+05	0.04	0.447	0.73	5.186	1.45	0.98	21.4	14.93	3.67	1.771	118	57	0.1811
33989	1E+05	0.05	0.644	0.56	8.027	1.538	1.11	22.6	16.73	3.76	1.98	121	63.7	0.1868
34113	1E+05	0.01	0.02	1.19	0.998	1.617	0.02	23.7	1.792	3.93	0.006	127	0.17	0.187
34238	1E+05	0.03	0.358	0.9	3.899	1.656	0.94	24.2	14.4	4.02	1.739	129	56	0.1872
34362	1E+05	0.02	0.592	0.98	7.271	1.629	1.33	23.8	19.73	3.9	2.065	126	66.4	0.1899
34487	1E+05	0.03	0.319	0.81	3.322	1.637	0.9	23.9	13.85	3.95	1.73	127	55.7	0.1885
34611	1E+05	0.03	0.13	0.87	0.59	1.582	0.21	23.2	4.368	3.78	0.473	122	15.2	0.1905
34736	1E+05	0.04	0.015	0.71	1.074	1.59	0.01	23.3	1.685	3.7	0.006	119	0.17	0.1956

REFERENCES

Byers, J. P. (ed.), "Laboratory Evaluation of Metalworking Fluids," Metalworking Fluids, Marcel Dekker, Inc., New York, 1994, pp. 191-222.

Brinksmeier, E., and Werner, F., "Monitoring of Grinding Wheel Wear," Annals of the CIRP, Vol. 41/1, 1992, pp. 373-376.

Busch, D. M., and Prins, J. F., "A Basic Study of the Diamond Grinding of Alumina," in S. J. Schneider, Jr. and R. W. Rice (eds.), The Science of Ceramic Machining and Surface Finishing, NBS Special Publication 348, 1972, pp. 73-87.

Gagliardi, J. J., "Dynamics of Grinding Brittle Materials with Coated Abrasives," American Ceramic Society Ceramic Bulletin, Vol. 71, No. 11, 1992, pp. 1641-1646.

Gangopadhyay, A. K. and M. A. Tamor, "Friction and Wear Behavior of Diamond Films Against Steel and Ceramics," Wear, Vol. 169, 1993, pp.221-229.

Hahn, R. S., "Ceramic Grinding with Self-Sharpening Diamond Wheels," in S. Jahanmir (ed.), Machining of Advanced Materials, NIST Special Publication 847, U.S. Government Printing Office, Washington, DC, 1993, pp. 89-99.

Hu, K. X., and Chandra, A., "A Fracture Mechanics Approach to Modeling Strength Degradation in Ceramic Grinding Processes," Journal of Engineering for Industry, Transactions of the ASME, Vol. 115, 1993, pp. 73-84.

Hwang, T. W., "Analysis of Surface Quality in Machining of Metals and Advanced Ceramics," Ph. D. Thesis, University of Maryland, College Park, MD, 1992, pp. 112-115.

Inasaki, I., "Dressing of Resinoid Bonded Diamond Grinding Wheels," Annals of the CIRP, Vol. 38/1, 1989, pp. 315-318.

Inasaki, I., Tonshoff, H. K., and Howes, T. D., "Abrasive Machining in the Future," Annals of the CIRP, Vol. 42/2, 1993, Keynote Papers.

Ives, L. K., Evans, C. J., Jahanmir, S., Polvani, R. S., Strakna, T. J., and Mcglauflin, M. L., "Effect of Ductile-Regime Grinding on the Strength of Hot-Isostatically-Pressed Silicon Nitride," in S. Jahanmir (ed.), Machining of Advanced Materials, NIST Special Publication 847, U.S. Government Printing Office, Washington, DC, 1993, pp. 341-352.

Ives, L. K., and Jahamnir, S., "Grinding Optimization for Advanced Ceramics," in Sixth Program Review Meeting, NIST, Gaithersburg, MD, 1995.

Jahanmir, S., Strakna, T. J., Quinn, G. D., Kopp, R. N., Yoon, S. C., and Kumar, K. V., "Effect of Grinding on Strength and Surface Integrity of Silicon Nitride: Part II," in S. Jahanmir (ed.), Machining of Advanced Materials, NIST Special Publication 847, U.S. Government Printing Office, Washington, DC, 1993, pp. 279-291.

Jahanmir, S., Strakna, T. J., Quinn, G. D., Liang, H., Allor, R. L., and West, R. D., "Effect of Grinding on Strength and Surface Integrity of Silicon Nitride: Part I," in S. Jahanmir (ed.), Machining of Advanced Materials, NIST Special Publication 847, U.S. Government Printing Office, Washington, DC, 1993, pp. 263-277.

Kalpakjian, S., Manufacturing Processes for Engineering Materials, Addison-Wesley Publishing Company, Reading, MA, 1991, pp. 589-605.

Kirk, J. A., "An Evaluation of Grinding Performance for Single and Polycrystal Grit Aluminum-Oxide Grinding Wheels," Journal of Engineering for Industry, Transactions of the ASME, Vol. 98, Series B, No. 1, 1976, pp. 189-195.

Kitajima, K., Cai, G. Q., Kumagai, N., Tanaka, Y., and Zheng, H. W., "Study on Mechanism of Ceramics Grinding," Annals of the CIRP, Vol. 41/1, 1992, pp. 367-371.

Konig, W., Steffens, K., and Ludewig, T., "Single Grit Tests to Reveal the Fundamental Mechanism in Grinding," in R. Komanduri and D. Maas (eds.), Milton C. Shaw Grinding Symposium, PED-Vol. 16, ASME, 1985, pp. 141-154.

Lindsay, R. P., and Hahn, R. S., "On the Basic Relationships between Grinding Parameters," Annals of the CIRP, Vol. 19, 1971, pp. 657-666.

Malkin, S., Grinding Technology: theory and applications of machining with abrasives, Ellis Horwood Limited, New York, 1989.

Malkin, S., and Cook, N. H., "The Wear of Grinding Wheels: Part 1 -- Attritious Wear," Journal of Engineering for Industry, Transactions of the ASME, Vol. 92, Series B, No. 1, 1970, pp. 1120-1128.

McEachron, R., and Lorence, S., "Superabrasive and Structural Ceramics in Creep-Feed Grinding," American Ceramic Society Ceramic Bulletin, Vol. 67, No. 16, 1988, pp. 1031-1036.

Mayer J. E., and Fang, G. P., "Effect of Grit Depth of Cut on Strength of Ground Ceramics," Annals of the Cirp, Vol. 43, No. 1, 1994, pp. 309-312.

Ovri, J. E. O., and Davies, T. J., "Effect of Surface Condition on the Flexural Strength of Sintered Silicon Nitride," Journal of Materials Science Letters, Vol. 6, 1987, pp. 849-850.

Pai, D. M., Ratterman, E., and Shaw, M. C., "Grinding Forces and Energy for Brittle Materials," Intersociety Symposium on Machining of Advanced Ceramic Materials and Components, ASME, 1988, pp. 99-111.

Peters, J., Snoeys, R., and Decneut, A., "The Proper Selection of Grinding Conditions in Cylindrical Plunge Grinding," in C. Bhateja and R. Lindsay (eds.), Grinding Theory Techniques and Troubleshooting, SME, Dearborn, MI, 1982, pp. 107-114.

Spur, G., Stark, C., and Tio, T. H., "Grinding of Non-Oxide Ceramics Using Diamond Grinding Wheels," Machining of Ceramic Materials and Components, in K. Subramanian and R. Komanduri (eds.), PED-Vol. 17, ASME, 1985, pp. 33-43.

Story, R. W., "Forces and Force Ratios in Grinding With Coated Abrasives," Journal of Engineering for Industry, Transactions of the ASME, Vol. 90, Series B, No. 1, 1968, pp. 407-410.

Subramanian, K., and Keat, P. P., "Parametric Study on Grindability of Structural and Electronic Ceramics -- Part 1," in K. Subramanian and R. Komanduri (eds.), Machining of Ceramic Materials and Components, PED-Vol. 17, ASME, 1985, pp. 25-32.

Subramanian, K., Redington, P. D., and Ramanath, S., "A Systems Approach for Grinding of Ceramics," in S. Jahanmir (ed.), Machining of Advanced Materials, NIST Special Publication 847, U.S. Government Printing Office, Washington, DC, 1993, pp. 43-53.

Tricard, M., Norton Company, Worcester, MA, personal communication, 1995.

Tsutsumi, C., Okano, K., and Suto, T., "High Quality Machining of Ceramics," Journal of Materials Processing Technology, Vol. 37, 1993, pp. 639-654.

Verkerk, J., "Wheel Wear and Forces in Surface Grinding," Annal of the CIRP, Vol. 23, 1974, pp. 81-82.

Xu, H. K., Jahamnir, S., and Ives, L. K., "Effect of Grinding Damage on Fracture Strength of SRBSN and Zirconia," in Eighth Program Review Meeting, NIST, Gaithersburg, MD, 1996, pp. 12-35.

Xu, H. K., National Institute of Standards and Technology, Gaithersburg, MD, personal communication, 1996.

Yoshikawa, H., and Sata, T., "Study on Wear of Grinding Wheels: 1, Bond Fracture in Grinding Wheels," Journal of Engineering for Industry, Transactions of the ASME, 1963, pp. 39-43.